Abstract (In Chinese)

基於扇形晶格設計具任意角度之光子晶體波導轉折

研究生 ： 施均融

指導教授 ： 李柏璁 教授

國立交通大學光電工程學系顯示科技研究所碩士班

摘要

光子晶體的研究中, 光在光子晶體波導中經過轉折後的能量散失一直是個很大的問題. 許多研究都在想辦法改善這個問題. 目前爲止已經提出許多的方法來改善波導轉折的能量散失, 但是都是在 60 度或 120 度這些特別角上面做改善. 在任意角度下波導轉折能量散失的研究卻不多見.

在這篇論文中, 我們結合了圓形光子晶體跟環型布拉格反射鏡的概念做出了可以彎曲任意角度的光子晶體波導, 並且我們調整波導的寬度使波導在通訊的波段上有低損耗且寬頻的特性. 也用二維有限時域差分法模擬的方式證明了我們的結構在 60 度到 120 度都可以有相同的高傳輸率頻帶. 元件也可以成功的被製造出來. 我們也用間接與直接的方法去量測我們的元件.

Abstract (In English)

Arbitrary Photonic Crystal Waveguide Bend Based on Sector-Shaped Lattice Cell

Student: Chun-Jung Shih

Advisor: Prof. Po-Tsung Lee

National Chiao Tung University

Department of Photonic & Display Institute

Abstract

In the research of photonic crystal, photonic crystal waveguide bending loss is always a big problem. There are many studies to improve it. Lots of methods are proposed to improve the bending loss, but usually in special angle like 60° or 120°. The research of arbitrary waveguide bending loss is rarity.

In the thesis, we combine the concepts of circular photonic crystal and annular bragg reflector to design a arbitrary waveguide bend, and optimizing the waveguide width achieve low loss and with broad bandwidth at communication wavelength. We also using 2D FDTD simulate our structure in possession of the same high transmission band at 60°~120°. The device has fabricated, and measures it by direct and indirect method.

Acknowledgement

我的求學的路途到這裡總算是告一段落了，這一路上要感謝的人實在是太多了，但是首先最感謝的還是我的父母，他們讓我在 18 年的求學生涯中能夠無憂無慮的將心思都放在課業上，也讓我自由的選擇自己將來要走的路。也很感謝從大三一直陪伴我到現在的女朋友，藍藍，總是在我實驗不順利的時候給我鼓勵，陪我去拜土地公，還常常辛苦的台北新竹兩地跑，還拜託你父親幫我看我論文的英文文法。沒有你們我就不會有現在的成就。

接下來我也要感謝我的指導老師李柏璁教授，在研究所這兩年不斷的為我指點迷津，指引我研究的方向，也不厭其煩的協助我解決研究上的瓶頸，除此之外也幫助我在研究所之後的生涯規劃。還要感謝實驗室的博班學長盧贊文，在研究內容與量測系統的架設上給我相當大的幫助。還有實驗室的同學老漢，嘴，大孟姐跟璁哥，互相的吐槽跟嘴砲讓枯燥的實驗變的有趣許多，此外還要感謝蕭逸華，何韋德，周香君，李欣育，洪青樺跟林怡先學弟妹們的幫助，常常幫我寫 E-BEAM 跟吃 ICP，讓我能夠順利的將元件作出來

2008/10/06　于新竹 國立交通大學　交映樓 415 室　PC124

Content

List of Figure

Chapter 1. Introduction

1.1. Introduction to photonic crystal

In 1987, Yablonovitch has produced the structure of photonic crystal [1-3]. In a word, the structure of photonic crystal is to arrange the dielectric in a periodically, so that part of the light will not transmit after multiple scattering in the periodical structure. By using this method we can confine the light in some region we want. We call this photonic bandgap (PBG). At first Yablonovitch wanted to improve the spontaneous emission loss from laser, he thought using photonic bandgap around atoms and decreasing the loss from laser. Then, the research of photonic crystal grew quickly and had become close to our lives. Now, photonic crystal has been used in many areas, like photonic crystal LED, photonic crystal fiber…etc. The diagrams of the 1D, 2D and 3D's are illustrated in Fig.1.1.[3]

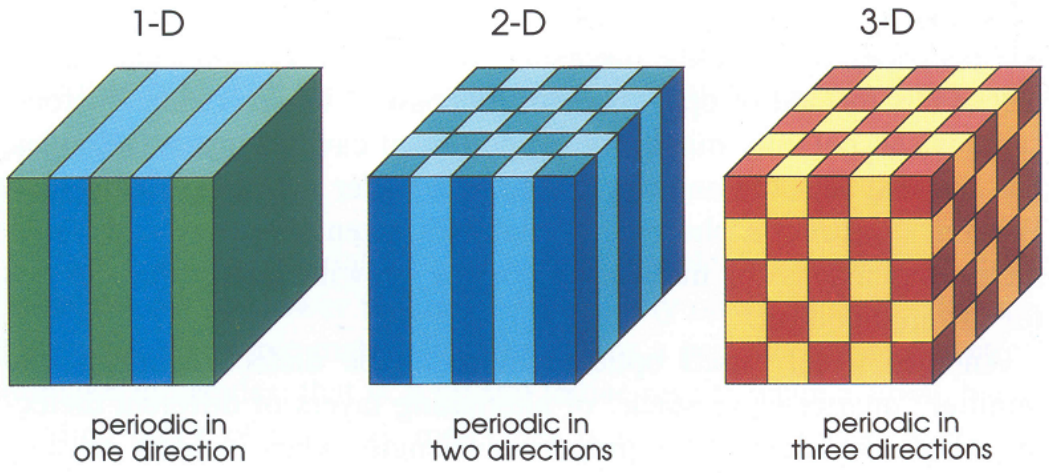

Fig.1.1 Simple examples of one-dimension, two-dimension, three-dimension photonic crystals, where different colors represent different dielectric constant of material [3]

First, one dimension photonic crystal is using different materials stacked up layer by layer, so it can enhance transmission or reflection of certain band of light

wavelength and it is used generally in our lives [4-5], for example, multi-films of glasses, which can enhance the transmission of visible light and reflection of ultraviolet to protect our eyes, reflection mirror in semiconductor laser…etc

Then, two kinds of materials arrayed periodically in two dimensions are called "two dimension photonic crystal". In fact, the structure of a 2D photonic crystal is divided as hole in dielectric and rod in air. The patterns of array include mainly rectangular and triangular (Fig 1.2) [3]. The other patterns are quasi and circular ones. In general, the structure of the hole in dielectric is generally arranged in the triangular pattern to obtain large bandgap for TE mode, and the rod in air is in the rectangular pattern to obtain large bandgap for TM mode, which is shown in Fig 1.3 [3]. So in in-plane direction we can confine light by PBG. Moreover, we usually use index confinement to confine light in vertical direction. For this reason, 2D photonic crystal is usually fabricated on membranes structures.

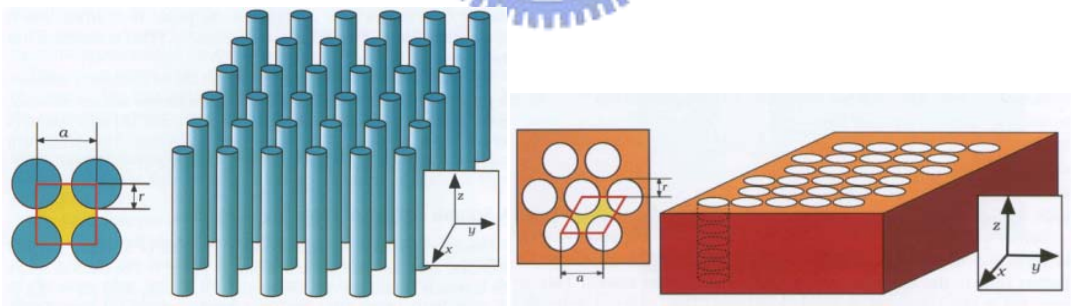

(a) (b)

Fig.1.2 (a) rectangular lattice with rod in air structure (b) triangular lattice with hole in dielectric structure [3]

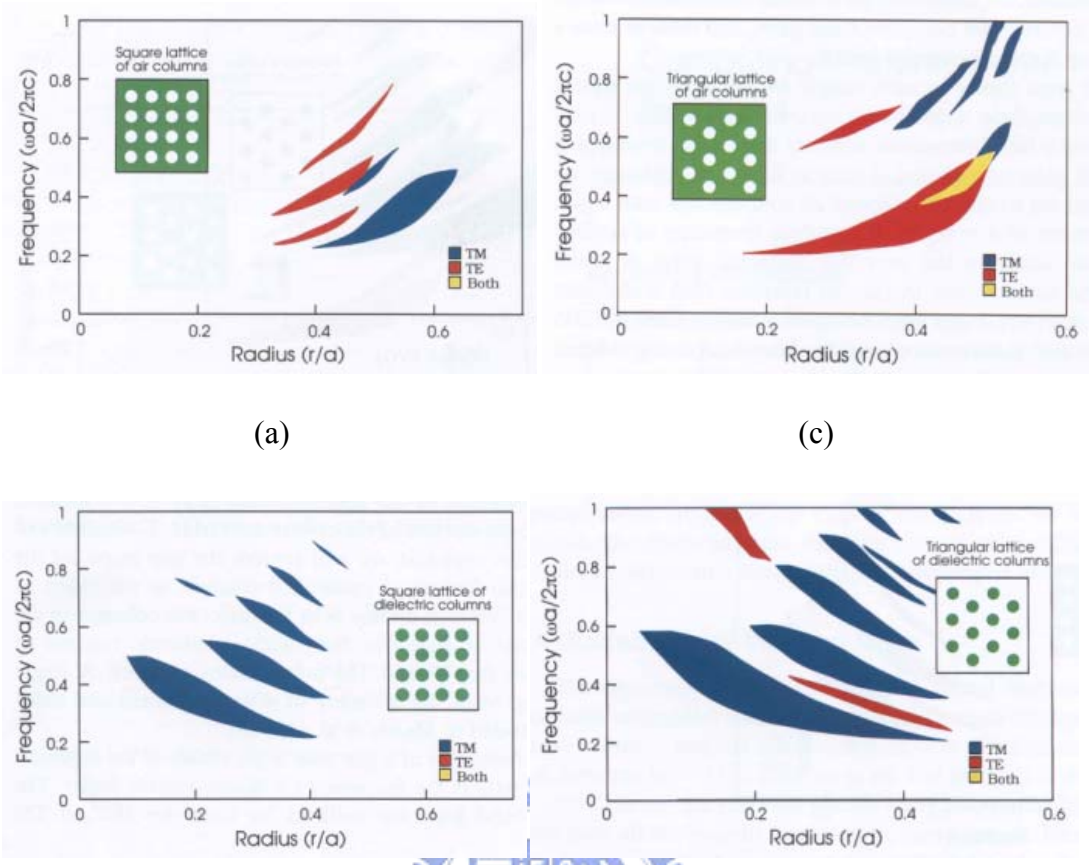

Fig.1.3 bandmap for rectangular lattice of (a) hole in dielectric (b) rod in air; triangular lattice of (c) hole in dielectric (d) rod in air[3]

Finally, the 3D photonic crystal is with a complete bandgap (both TE and TM mode). But the fabrication and simulation of 3D photonic crystal is more complex than 2D or 1D photonic crystal. In general, fabrication in 3D photonic crystal is piled as nano-rod or nanometer ball. However, to create a cavity or waveguide on photonic crystal is easier in 2D photonic crystal; so most studies are in the 2D area.

1.2. Photonic Crystal Waveguide and Bend

In the previous section, we introduce the characteristic of PBG of photonic crystal. Parallel to semiconductor, making defect can create defect mode in photonic

crystal. In photonic crystal, a waveguide can be created by a line defect; we call it "photonic crystal waveguide" which was first fabricated by J.D. Joannopoulos in 1988 [6]. Fig1.4 shows a single line defect waveguide and its propagation mode (defect mode). The researches of photonic crystal waveguides are very extensive; the topics include many developments such like photonic crystal waveguide bend[7-13], coupling properties of photonic crystal waveguide[14-17], power-splitter photonic crystal[18], photonic hetero- structure waveguide[19-21]…etc. Because of PBG, photonic crystal waveguide can confine light better than traditional index guiding waveguide.

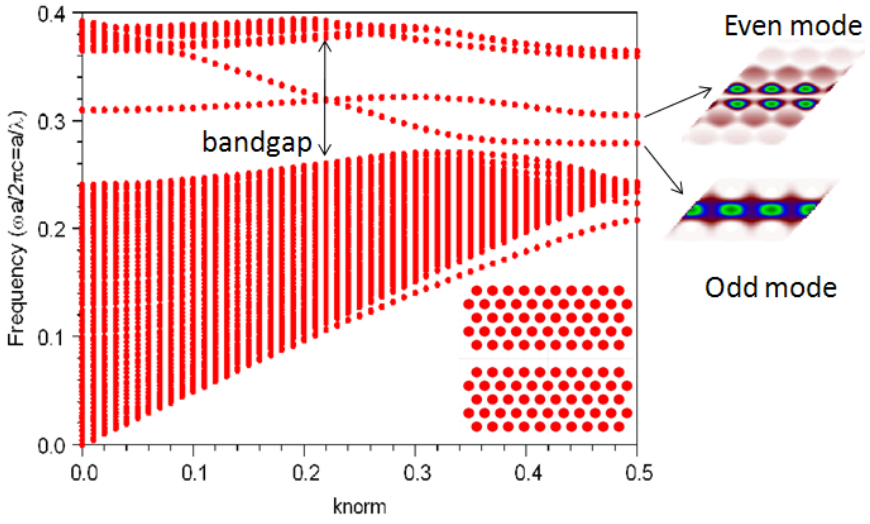

Fig.1.4 photonic crystal waveguide by removing a row of holes and its propagation mode

Photonic crystal waveguide formed by line defects in 2D photonic crystal consisting of air holes of triangular lattice in dielectric slabs are more commonly fabrication, but high transmissions (over 90%) through direct sharp bends can only be achieved for light waves in a frequency range limited to 9% of the central frequency [15]. Consequently, studies have been focused on optimizing the bend structures to improve the transmissions. Prominent solutions include moving a unit cell of the bends (Fig.1.5 (a)) [7], using defects to make the bends single mode (Fig.1.5 (b)) [8],

incorporating taper structures into the bends (Fig.1.5 (c)) [9], and making elaborate topology optimizations on the 60° and 120° bends (Fig.1.5(d)(e)) [10]. However, in most of the previous works, high transmissions were obtained at the expense of shortness or sharpness of the bends. At present, topology is used to optimize the bend loss expensively. Fig1.6 shows 60° and 120° bends with topology optimization which published on Optical Letter in 2007. In this paper, high transmission (over 90%) bandwidth is 101nm and 74nm for 60° and 120° respectively [11].

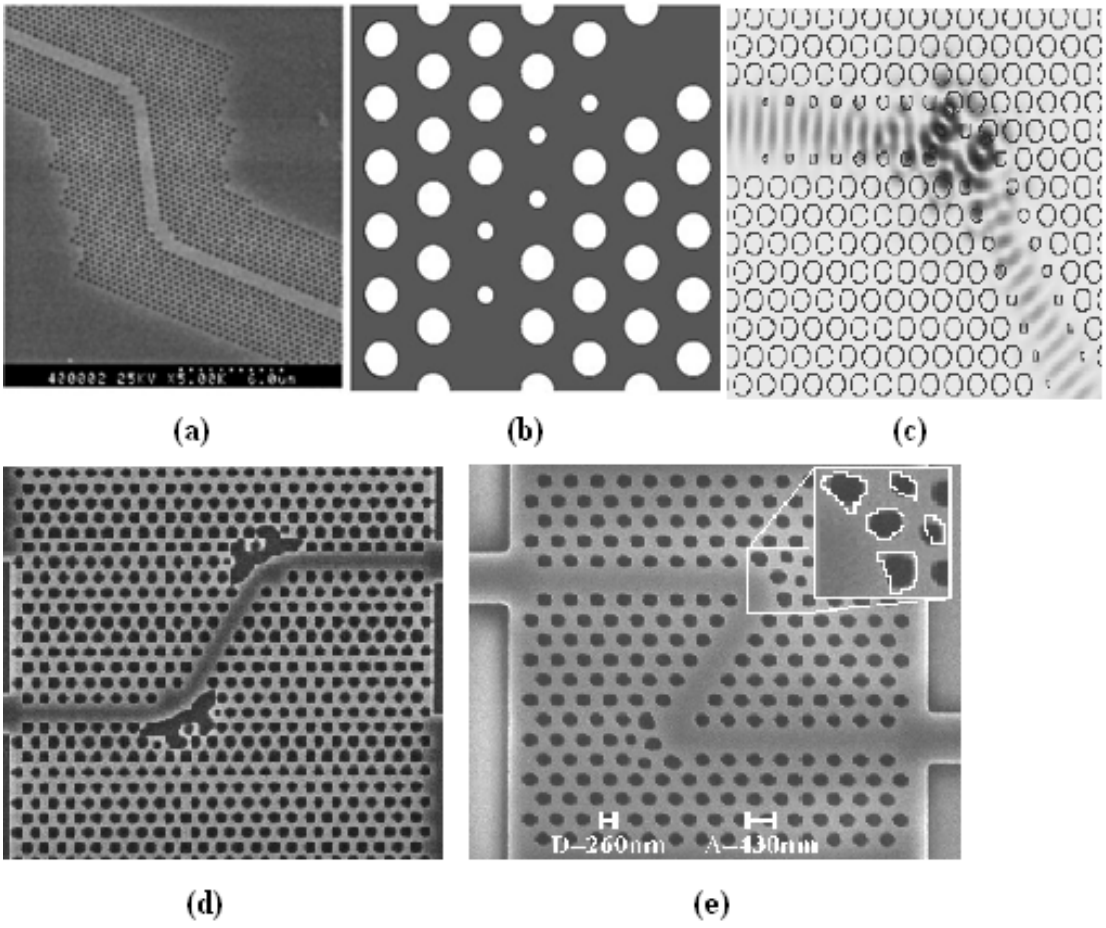

Fig.1.5 (a) moving a unit cell of the bends[7] (b) using defects to make the bends single mode [8] (c) incorporating taper structures into the bends[9] (d) (e) making elaborate topology optimizations on the 60° and 120° bends[10]

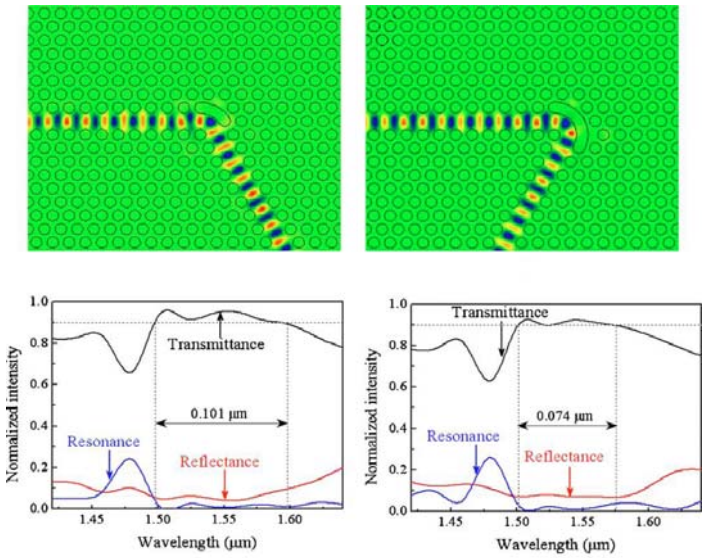

Fig.1.6 60° and 120° bend with topology optimization and transmission spectrum[11]

1.3. Circular photonic crystal

Although 60° and 120° bends have already been researched by many groups and greatly reduce the reflection loss and widened the high-transmission bandwidths, bend of the other angle have not be researched as much as those of 60° and 120° bends. In 2005, H.Miyazaki group using 5-fold symmetrical circular photonic crystal presented 72° waveguide bending with rod in air rectangular lattice structure for microwave [12]. The lattice position in x-y plane is given by Eq.1 and the figure show in Fig.1.7. In the same year, Sanshui Xiao group studied transmission properties for waveguide bends by use of a circular photonic crystal with hole in dielectric triangular lattice structure [13]. The result shows the high transmission bandwidth relates to the curvature of circular photonic crystal as shown in Fig.1.8.

$$x = dN\sin(\frac{2m\pi}{6N}),\ y = dN\cos(\frac{2m\pi}{6N}) \quad \ldots \text{Eq.1}$$

d= $\sqrt{3}$ a/2, N, d, and m denote the number of concentric circles, the difference of radii of neighboring concentric circles and the number of air holes ($0 \le m \le 6N$),respectively

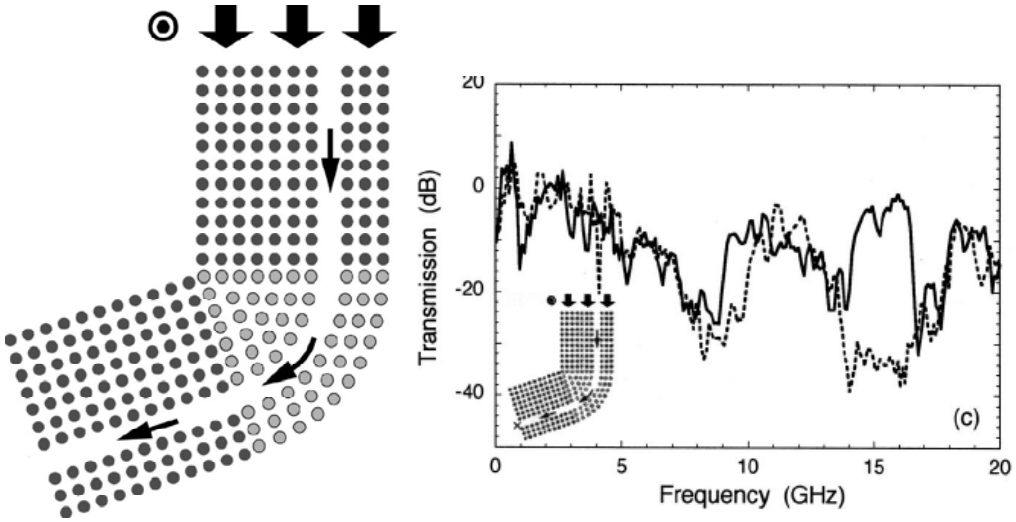

Fig.1.7 5-fold symmetrical circular photonic crystal present 72° waveguide bending with rod in air rectangular lattice structure

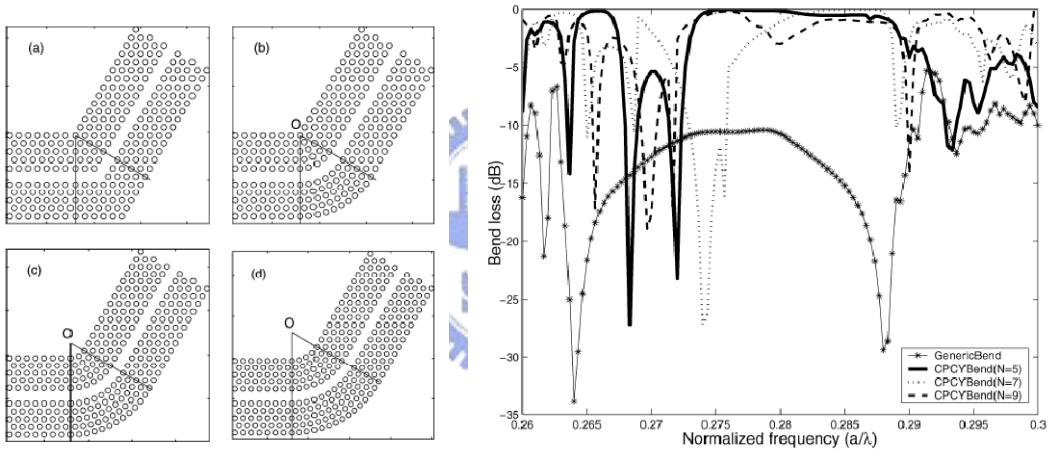

Fig.1.8 transmission properties for waveguide bends by use of a circular photonic crystal with hole in dielectric triangular lattice structure

We can find less and less high transmission band width as N increases. Because is it that the outer layer of circular photonic crystal looks like rectangular lattice structure. We have known that hole in dielectric structure is with narrow bandgap when lattice structure is rectangular. Althogh circular photonic crystal has been acheievd waveguide bend in the other angle, it has still some problems. One is poor bandgap, the other is not really arbitrary.

1.4. Annular bragg reflection

In last section, we introduce circular photonic crystal. Because it's poor bandgap, we can't use it to take as not waveguide bend but ring cavity. In the reasearch of ring cavity, light confinement of annular bragg reflection is better than circular photonic crystal [22, 23]. The design is shown in Fig.1.9 [22]. Generally speaking, annular bragg reflection is dielectric arrangement in radial direction. Although light confinement of annular bragg reflection is better than circular photonic crystal, we can't fabricate it on membrane structure. However, if we use this structure to replace circular photonic crystal in waveguide bend region. We can really achieve arbitrary waveguide bend.

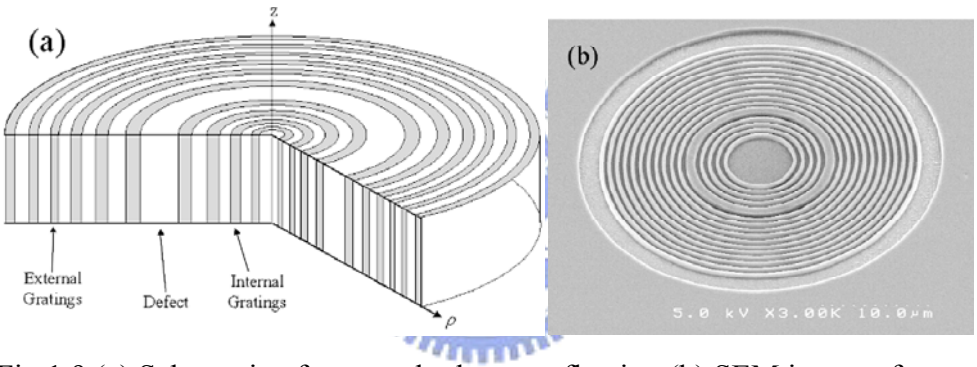

Fig.1.9 (a) Schematic of an annular bragg reflection (b) SEM image of an annular bragg reflection

1.5. Motivation

In photonic crystal research area, most research focus on 60° and 120° waveguide bend. Arbitrary angle waveguide bending hasn't been realized, and circular photonic crystal has bad transmission properties when be used in waveguide bending. In order to realize the photonic integrated circuit, waveguide bends play an important role. If broad bandwidth arbitrary bending be achieved, it is helpful to realize photonic integrated circuit. We will combine circular photonic crystal and annular bragg reflector to realize high transmission(less than 3dB) for arbitrary angle waveguide

bending with over 100nm bandwidth, and optimize its structure letting the center of bandwidth at communication wavelength .

Chapter 2. Simulation

2.1. The numerical methods used in photonic crystal simulation

In this section, we introduce the theory of numerical methods used in photonic crystal simulation. We begin with the Maxwell equations, which are basic equation for light propagating in the free space and media. Then, we will introduce plane wave expansion (PWE) and finite difference time domain (FDTD), the two important numerical methods in photonic crystal.

$$\nabla \bullet D = 4\pi\rho$$
$$\nabla \bullet B = 0$$
$$\nabla \times E = -\frac{1}{c}\frac{\partial B}{\partial t} \quad \text{…Eq.2}$$
$$\nabla \times H = \frac{1}{c}\frac{\partial D}{\partial t} + \frac{4\pi}{c}J$$

At first, light propagating will obey the Maxwell equation as show above in Eq.2, where E, H, D and B represent the electric field, magnetic field, displacement field and magnetic flux density corresponsively, and c is light speed in vacuum. The definitions of D and H are:

$$D = \varepsilon(r)E + P$$
$$H = \frac{B}{\mu(r)} - M \quad \text{…Eq.3}$$

where P is polarization vector(C/m^2), and M is magnetization vector (A/m^2).In general, ε and μ are the function of location and cannot be removed outside of the ▽ operator. Now if we only consider the dielectric and nonmagnetic medium, then μ is independent of space and is a constant equal to $4\pi\times10^{-7}$ and M is equal to 0. The form of D field is more complex because the polarization vector is not only the function of space but also the function of E field. The formula D is:

$$\tilde{P}(t) = \chi^{(1)}\tilde{E}(t) + \chi^{(2)}\tilde{E}^2(t) + \chi^{(3)}\tilde{E}^3(t) + \ldots$$
$$D_i = \sum_j \varepsilon_{ij} E_j + \sum_j k\chi_{ijk} E_j E_k + O(E^3) \quad \ldots\text{Eq.4}$$

The ~ above P and E represents they are scalar fields. However, we usually assume the intensity of excitation light is smaller enough so that the nonlinearity can be ignored. If we further assume that the material is isotropic and homogeneous in all space, the D field can be simply reduced to the form:

$$D(r) = \varepsilon_0 \varepsilon_r(r) E(r) \quad \ldots\text{Eq.5}$$

Then we put Eq.5 in Eq.2 to replace the D field and do some curl operation and substitution, we can get the wave equation in source free region:

$$\Theta_E \vec{E}(\vec{r}) = \frac{1}{\varepsilon(\vec{r})} \nabla \times \{\nabla \times \vec{E}(\vec{r})\} = \frac{\omega^2}{c^2} \vec{E}(\vec{r})$$
$$\Theta_H \vec{H}(\vec{r}) = \nabla \times \left\{\frac{1}{\varepsilon(\vec{r})} \nabla \times \vec{H}(\vec{r})\right\} = \frac{\omega^2}{c^2} \vec{H}(\vec{r}) \quad \ldots\text{Eq.6}$$

Eq.6 is the eigenvalue problems. Both Θ_E and Θ_H are Hermitian operators, so the eigenvalue ω^2/c^2 and eigenvectors $\vec{E}(\vec{r})$ and $\vec{H}(\vec{r})$ are real number and can be solved by numerical method.

Then, we introduce a method to calculate the band diagram for photonic crystal. It is named “Plane Wave Expansion” (PWE). This method is similar to the way to deal with the behavior of an electron (Kronig-Penney Model) in the periodic potential in solid-state physics. The periodic potential U(r) can be expressed as a complex fourier series (Eq.7) by using the reciprocal lattice vector ($\vec{G}$) where U(r) is the periodic potential. Similarly, the wave function of electron $\psi_k(r)$ in periodic potential can also be expanded by the plane waves which belong to complete set of Schrödinger

equation (Eq.7).

$$U(r) = \sum_G U_G e^{i\vec{G}\bullet\vec{R}}$$
$$\varphi_k(r) = \sum_G C(k-G) e^{i(\vec{k}-\vec{G})\bullet\vec{R}} \quad \ldots \text{Eq.7}$$

For the same reason, periodic dielectric distribution can also be expanded by reciprocal lattice vector (Eq.8) and the wave function of photon in periodic dielectric distribution can also be expanded by the plane waves which belong to the complete set of wave equation (Eq.8).

$$\varepsilon(r) = \sum_G \varepsilon_G e^{i\vec{G}\bullet\vec{R}}$$
$$\psi_k(r) = \sum_G M(k-G) e^{i(\vec{k}-\vec{G})\bullet\vec{R}} \quad \ldots \text{Eq.8}$$

Finally, we substitute the equation Eq.8 into Eq.6; we will get new wave equation:

$$(\vec{k}+\vec{G})\bullet(\vec{k}+\vec{G}')\times E_{G'} = -\omega^2 \sum_{G'} \varepsilon_{G,G'} E_{G'} \quad \ldots \text{Eq.9}$$

This equation can be expressed as a matrix form and the dispersion relation can be solved. The wavevector k is arbitrary, but can be replaced by k in the first Brillouin zone which is due to the translational symmetry inhered in photonic crystal. Therefore, we can limit our calculation in the first Brillouin zone. The $\varepsilon_{G,G'}$ is the Fourier coefficient of $\varepsilon(r)$ and $\varepsilon^{-1}(r)$, which is concerned with $G-G'$. All band diagrams of photonic crystal in this paper are calculated by this method. At first, we should define a supercell which is similar to the unit cell in solid crystal. The supercell of this band diagram is shown in Fig.2.1 (a). It should be kept in mind that the configuration of photonic crystal can always be expanded by the defined supercell. Fig. 2.1(b) is a typical TE band diagram for triangular lattice photonic crystal calculated by PWE

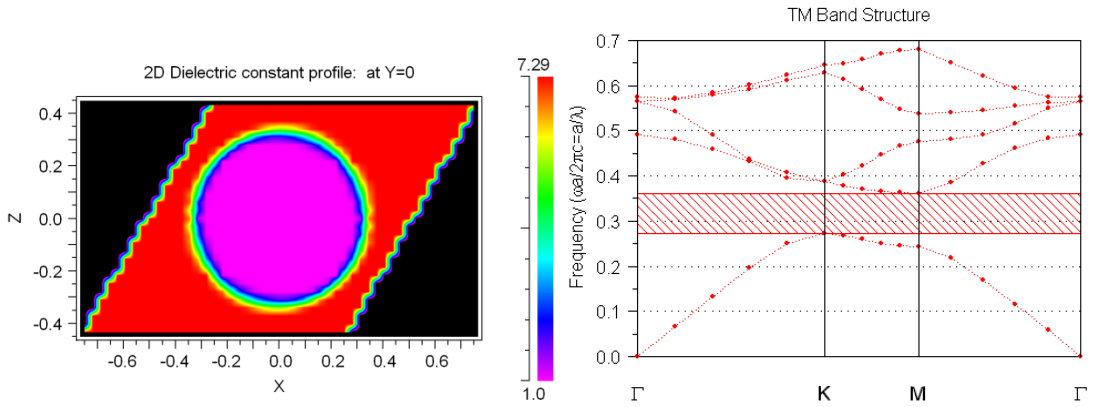

(a) (b)

Fig.2.1 (a) The supercell used in the simulation (b) The TM band diagram of triangular lattice photonic crystal with r=0.33a

Finally, we introduce finite-difference time-domain (FDTD) which is the method we used to calculate transmission spectrum of waveguide bend. Defect engineering is an important issue in designing the photonic crystal devices. However, although PWE method is applicable in calculating band structure, it cannot provide the time dependent behavior of light. As a result, the better way is to directly solve the Maxwell equation.

Maxwell equations are vector differential equations, but computers can only execute scalar addition or subtraction operations. Therefore, we should transform Maxwell equations into six scalar differential equations. FDTD Method is developed according to this ideal.

The six scalar differential equations for each field component of Faraday's law and Ampere's law are given by Eq.10, where s and σ donate the magnetic loss and conductivity.

$$\frac{\partial E_y}{\partial z}-\frac{\partial E_z}{\partial y}=(s+\mu_0\mu_r\frac{\partial}{\partial t})H_x$$

$$\frac{\partial E_z}{\partial x}-\frac{\partial E_x}{\partial z}=(s+\mu_0\mu_r\frac{\partial}{\partial t})H_y$$

$$\frac{\partial E_x}{\partial y}-\frac{\partial E_y}{\partial x}=(s+\mu_0\mu_r\frac{\partial}{\partial t})H_z$$

$$\frac{\partial H_y}{\partial z}-\frac{\partial H_z}{\partial y}=(\sigma+\varepsilon_0\varepsilon_r\frac{\partial}{\partial t})E_x \quad \text{…Eq.10}$$

$$\frac{\partial H_z}{\partial x}-\frac{\partial H_x}{\partial z}=(\sigma+\varepsilon_0\varepsilon_r\frac{\partial}{\partial t})E_y$$

$$\frac{\partial H_x}{\partial y}-\frac{\partial H_y}{\partial x}=(\sigma+\varepsilon_0\varepsilon_r\frac{\partial}{\partial t})E_z$$

In general case, distribution of refractive index is not uniform and may be dependent on the positions. Hence, in order to describe the distribution of refractive index in detail, all space are divided into many ideal grids, and each grid will be given one refractive index which is the average index for each grid.

The widely used grid form adopted in the FDTD is Yee cell as shown in Fig.2.2. In Yee cell, the electric fields are arranged on the edges of the cube, and the magnetic fields are centered on the facet, which is due to face that electric fields updated are induced midway during each time step between successive magnetic fields, and vice versa.

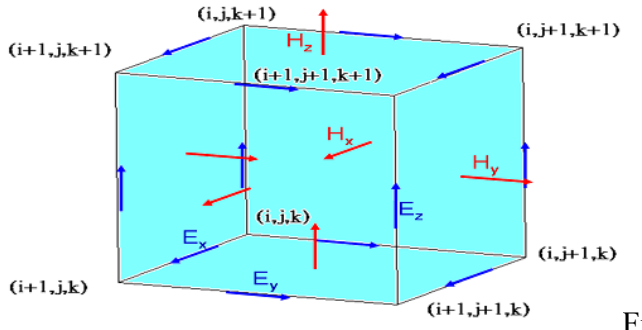

Fig2.2 The scheme of Yee cell

The index i, j, and k mark the positions of grid points in Cartesian coordinates. Therefore, the function of electric and magnetic field at the n_{th} time step can be expressed as $F(i\Delta x, j\Delta x, k\Delta x, n\Delta t) = F^n(x_i, x_j, x_k)$, where Δx is the increment of length and Δt is the increment of time step. The partial differential of six field components can be given as follow:

$$\begin{aligned}
\frac{\partial F^n(x_i,x_j,x_k)}{\partial x_i} &= \frac{F^n(x_{i+1/2},x_j,x_k)-F^n(x_{i-1/2},x_j,x_k)}{\Delta x} \\
\frac{\partial F^n(x_i,x_j,x_k)}{\partial x_j} &= \frac{F^n(x_i,x_{j+1/2},x_k)-F^n(x_i,x_{j-1/2},x_k)}{\Delta x} \\
\frac{\partial F^n(x_i,x_j,x_k)}{\partial x_k} &= \frac{F^n(x_i,x_j,x_{k+1/2})-F^n(x_i,x_j,x_{k-1/2})}{\Delta x} \\
\frac{\partial F^n(x_i,x_j,x_k)}{\partial t} &= \frac{F^n(x_i,x_j,x_k)-F^n(x_i,x_j,x_k)}{\Delta t}
\end{aligned} \quad \text{…Eq.11}$$

Furthermore, we substitute Eq.11 into Eq.10 and the six field components $E_x^{n+1/2}, E_y^{n+1/2}, E_z^{n+1/2}, H_x^{n+1/2}, H_y^{n+1/2}, H_z^{n+1/2}$ at the n+1/2 time step can be expressed with the field at the n_{th} time step. The detail mathematical expression can be found in reference 16. The distribution of whole electromagnetic wave can finally be obtained. Although this method can provided highly accurate results, it costs lots of computational resources. Hence, powerful parallel computation such as cluster is needed.

2.2. Annular bragg reflector bend

In chapter 1.4, we propose replacing circular photonic crystal in waveguide bend region to achieve arbitrary waveguide bend, like Fig.2.3 (a). The annular bragg reflection is dielectric arrangement in radial direction to become a omni-directional DBR. The considered PC structure is a dielectric slab with air holes of triangular

lattice. The thickness *h* of the slab and the radius *r* of the air holes are *h*=220nm and *r*=0.35*a*, respectively, where *a* is lattice constant. For operating at 1550nm, *a* is specified as *a*=510nm. Then, we create a line defect to be photonic crystal waveguide. To make the waveguide is single mode and even mode; we focus on 1400nm~1650nm. In the bend region, the width of air (*Wa*) and dielectric (*Wd*) in the bend region are 330nm and 112nm(see Fig.2.3(b)). It is not the design of DBR (λ/4), because we want to make the bend region to match the photonic crystal (period of annular reflection is the same as $\frac{\sqrt{3}}{2}$period of photonic crystal). We use 2D FDTD simulate the transmission spectrum when annular bragg reflector bend in 120° and refractive index set to 2.7. Before simulating transmission spectrum, we want to know the bandgap of annular bragg reflection of our design and also simulate it by FDTD. How we simulate bandgap by FDTD? We put an impulse source in blue circle and time monitor (green bar) at out of annular bragg reflection (see Fig.2.4(a)). After simulation we can get a spectrum Fig.2.4(b).

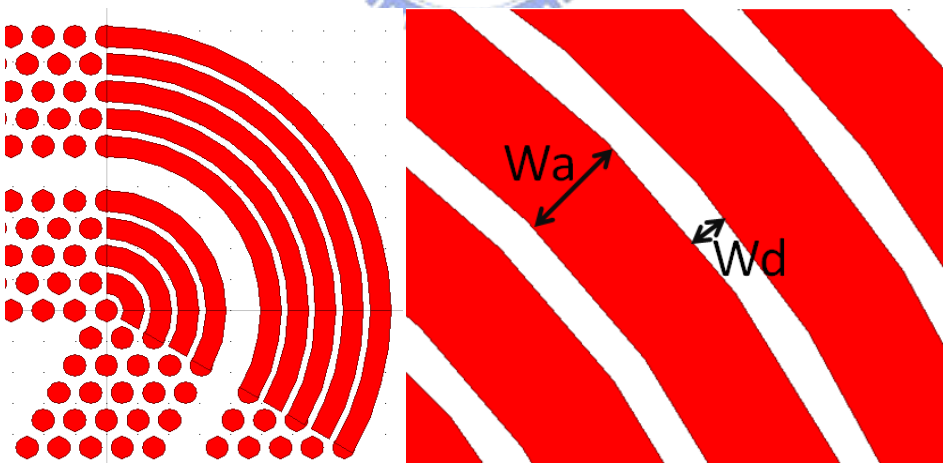

(a) (b)

Fig.2.3 (a) The 120° waveguide bend (b) two parameter of annular bragg reflection region

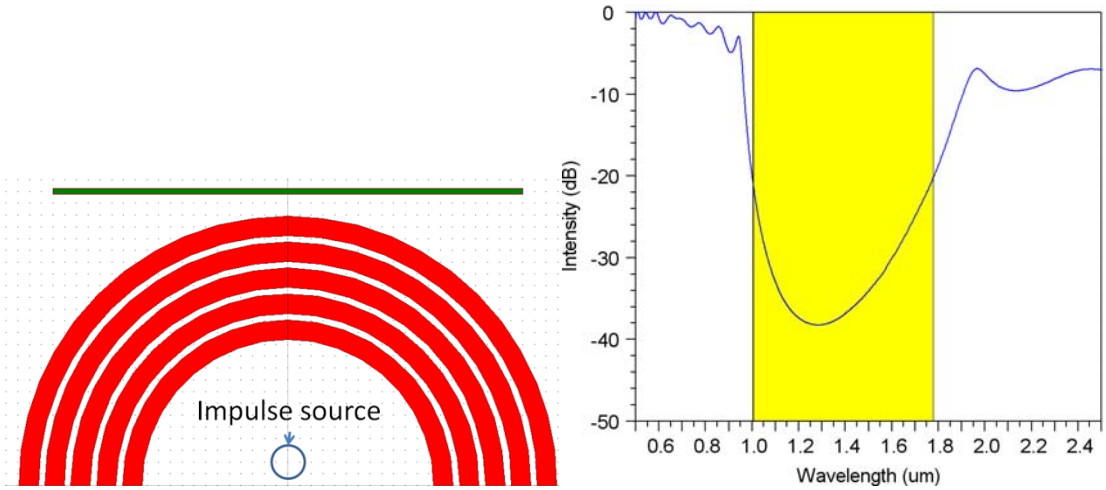

(a) (b)

Fig.2.4 (a)the configuration of FDTD simulation (b) the spectrum of FDTD simulation

In this thesis, we define bandgap when intensity less 20dB. So the bandgap of annular bragg reflection is from 1000nm to 1800nm (Fig.2.9 (b) yellow region). It overlaps the propagation wavelength which we want. We make sure the annular bragg reflection possessing bandgap which can confine light in bend region. Then we simulate the transmission spectrum of the structure which shows in Fig.2.5 (a) and the result show in Fig 2.7. We can find this structure possessing good transmission and broad bandwidth. We can achieve arbitrary waveguide bend by modulating the angle of annular bragg reflection, but this structure can't be fabricated on membrane structure. Because the width of dielectric layer (*Wd*) is too thin to hold in fabrication process. We try to modulate this structure to let it be fabricated on membrane structure.

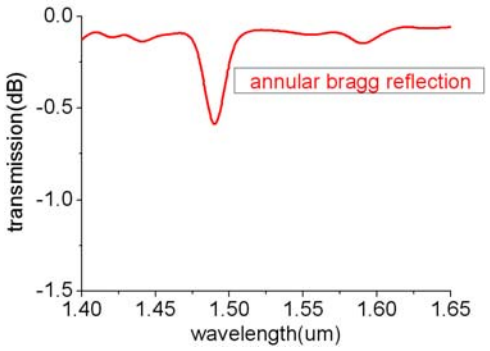

Fig.2.5 transmission spectrum of annular bragg reflection bend

2.3. Sector-shaped lattice cell

In last section, we find a problem in annular bragg reflection bend. So we try to modulate the annular bragg reflection and make it can be fabricated on membrane structure. We consider combining circular photonic crystal and annular bragg reflection. We divide the trench into several parts. The generic structure is shown in Fig.2.8. The arrangement of the sector defines the type of the reflector. Specifically, we focus on three different types of structures: the rectangular lattice (Fig. 2.6(a)), the triangular lattice (Fig. 2.6(b)) and the “sunflower” lattice (Fig. 2.6(c)) [16]. The rectangular lattice structure is a cylindrical counterpart of the rectangular photonic crystal in Cartesian coordinates. Each “necklace” consists of identical number of sector and the angular length of the sector increases for larger radii. The sectors in the triangular lattice structure are arranged in a similar way but with a half period shift in the azimuthal direction. The sunflower lattice structure comprises sectors of the same angular size where the number of sectors in each concentric ring is proportional to the circumference of the ring [24]. In this paper, the type we choose and discussion is sunflower structure. Because is it the size of sector of this structure is similar to each other. It is convenient to our fabrication.

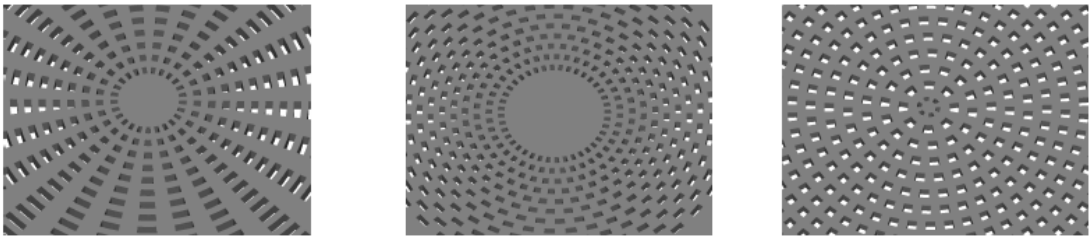

(a) (b) (c)

Fig.2.6 (a) rectangular structure (b) triangular structure (c) sunflower structure

So we combine circular photonic crystal and annular bragg reflection to let it like the flower structure. The illustration is shown in Fig.2.7 (a) and we define some parameter of flower structure (Fig 2.7(b) and (c)). In our design, θp,θw,θi and *Wa* are equal to 510nm, 357nm, 255nm and 330nm respectively. At first, we also use FDTD to simulate the bandgap of our structure of bend region. The result show in Fig2.8.The yellow region is the bandgap of our structure of bend region.

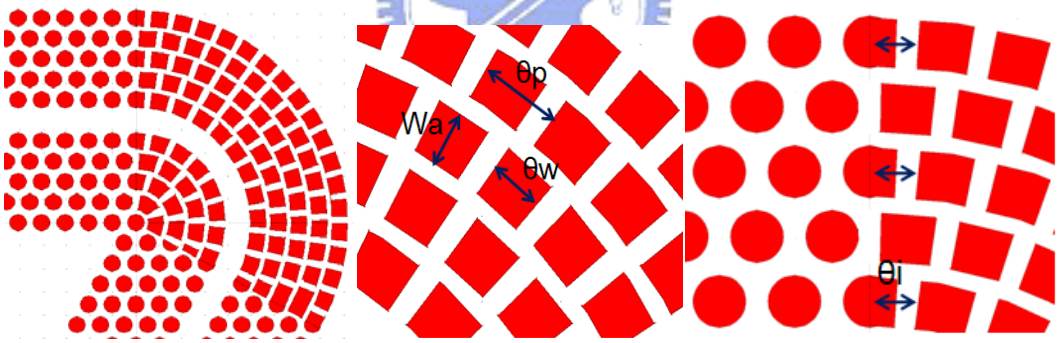

(a) (b) (c)

Fig.2.7 (a) the illustration of bent waveguide of reflector composed by sector and some parameter (b) some parameters definition

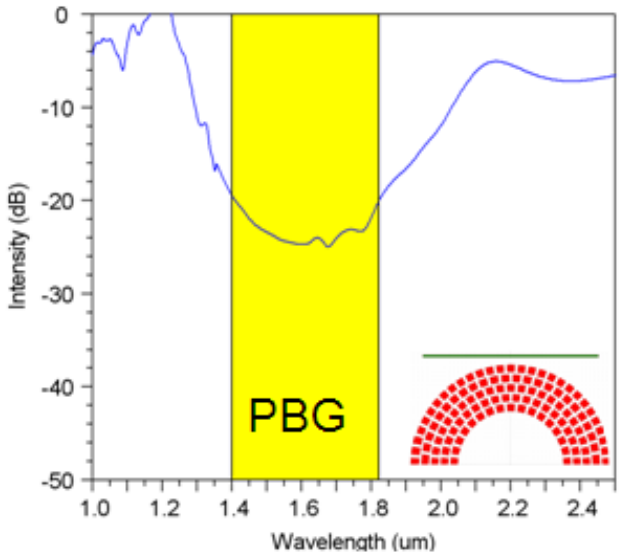

Fig.2.8the photonic bandgap of our structure of bend region

The bandgap of our structure of bend region is from 1400nm to 1820nm. Although the bandgap is narrower than annular bragg reflection, it still overlap the wavelength which we want. Then we simulate the transmission spectrum of the sector- shaped lattice cell bend. The result is shown in Fig.2.9. We can find two low transmission dips. If we solve low transmission region, high transmission bandwidth is about 300nm. To study reason of low transmission, we simulate resonant spectrum in bend region. The result show that two resonance peak exist at 1406nm and 1498nm, and compare with low transmission dips (Fig.2.10). We can find the space of low transmission dips and resonance peaks are match. So we can conclude that low transmission peak is due to resonance.

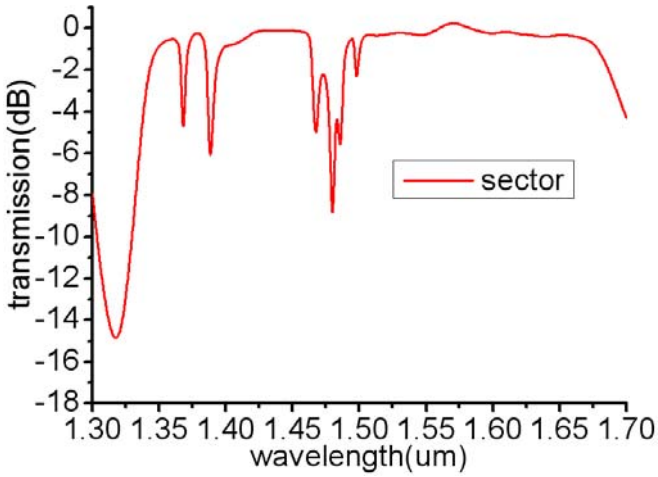

Fig.2.9 transmission spectrum of sector-shaped lattice cell waveguide bends

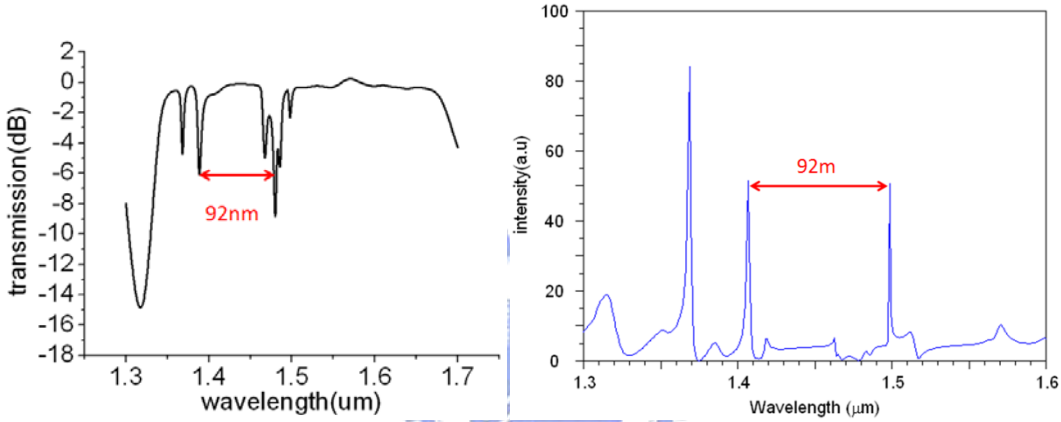

(a) (b)

Fig.2.10 (a) space width of low transmission peak (b) space between two resonance peaks

Next, we want to solve resonance effect in bent waveguide region. After seeing the resonance profile (Fig.2.11), we find the resonance profile looking like odd mode. To solve the problem of resonance, we can make some defect in bend region to destroy the resonance, but it also influence the transmission of waveguide bend. So we try to decrease bent waveguide width to make even mode blue shift. Because is there still a high transmission bandwidth from 1481nm to 1685 nm. If we move it to the wavelength which we want, it can still use in waveguide bend.

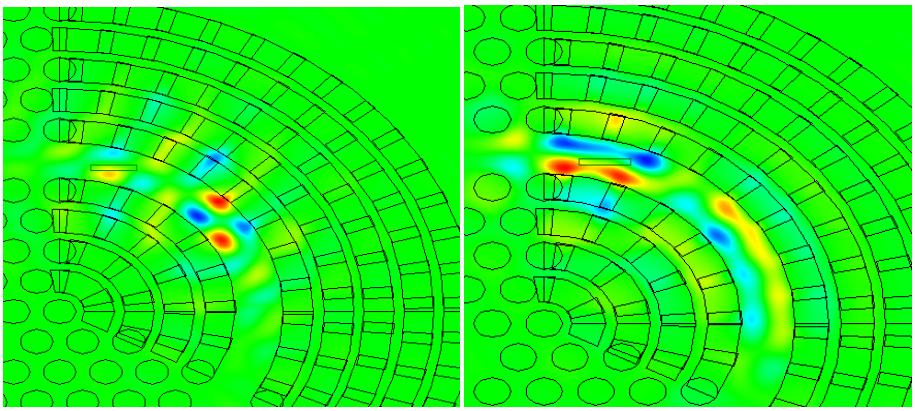

(a) (b)

Fig.2.11 resonance profile at (a) 1406nm (b) 1498nm

2.4. Modulate sector-shaped lattice cell and bend angle from 60° to 120°

In order to move transmission bandwidth to the wavelength which we want, we shift the green region of Fig.2.15 75nm to reduce the width of waveguide 75nm. Now the waveguide width in bend region is equal to 478nm. Then we simulate the transmission spectrum of it. The result is shown in Fig.2.12 (a). High transmission region is from 1424nm to 1641nm and bandwidth is equal to 217nm. It is clear that the bandgap is moving to the bandwidth which we want and we can observe from the plots in Fig.2.12 (a) that the power level at the output (blue) is almost the same as that at the input (green) of the waveguide bend.

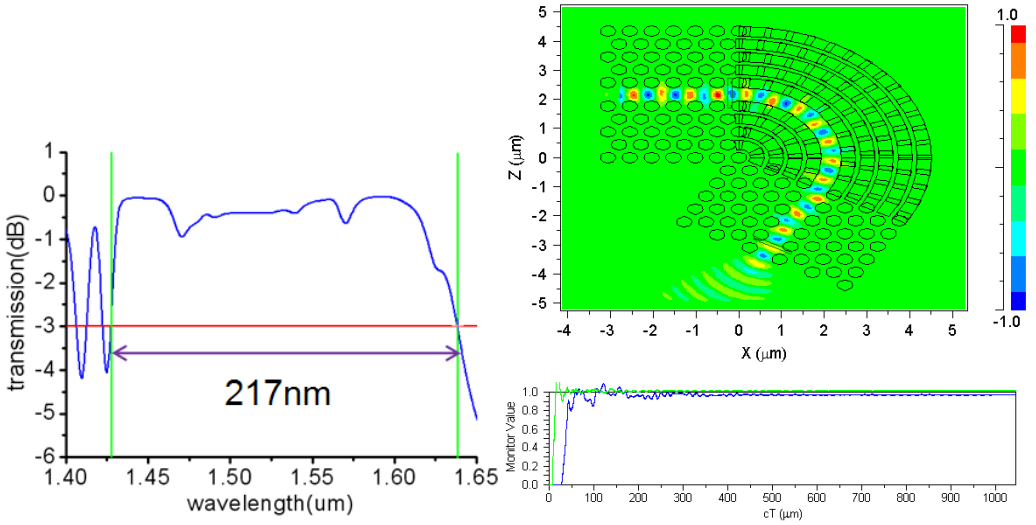

(a) (b)

Fig.2.12 (a) transmission spectrum when the width of waveguide bend region is equal to 478nm (b) Field evolution (upper) and monitored powers (lower) in the sector-shaped lattice cell waveguide bend

We have designed a sector-shaped lattice cell to achieve a broadband waveguide bend at 120°, but our goal is achieve arbitrary waveguide bend. So we use our design and make it bend at the other angle. Fig.2.13 show the 75° and 100° waveguide bend by using sector-shaped lattice cell, and then we simulate the transmission spectrum from 60° to 120°. The result is shown in Fig.2.14. We can find the bandwidth are almost over 200nm when waveguide bend at 60° and 120°, but the spectra are different when angles are different. So we make some issue of our structure.

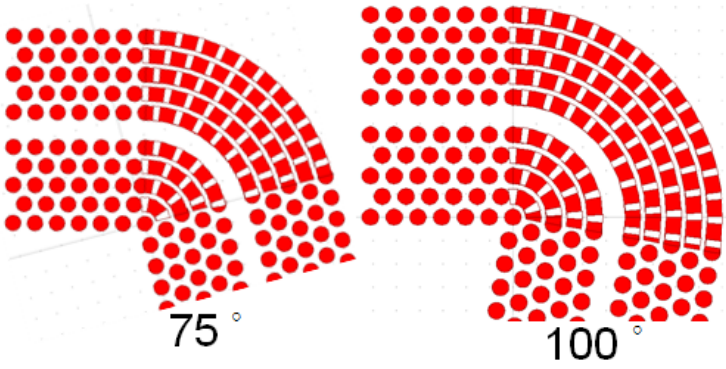

Fig.2.13 the schematic of waveguide bend at 75° and 100° by using sector-shaped

lattice cell

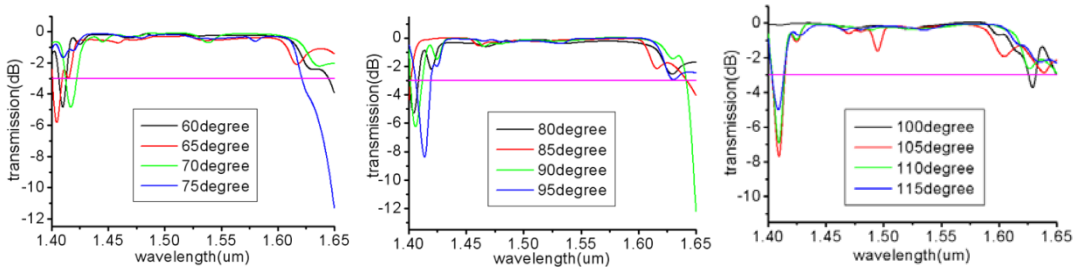

Fig.2.14 transmission spectra when waveguide bend from 60° to 120°

2.5. Sector-shaped lattice issue

In last section, we find the transmission spectra are different when angles are different. Obviously, our structure exist some different at different angle. In our design, the phase of sector-shaped lattice cell at the interface of waveguide bend region θ*i* is fixed, and the period of sector-shaped lattice cell *θp* is fixed too. In the end of the waveguide bend region are different at different angles, even if in the same angle, like Fig.2.15. Moreover, the spectra are different when the directions of propagation are different, like Fig.2.16

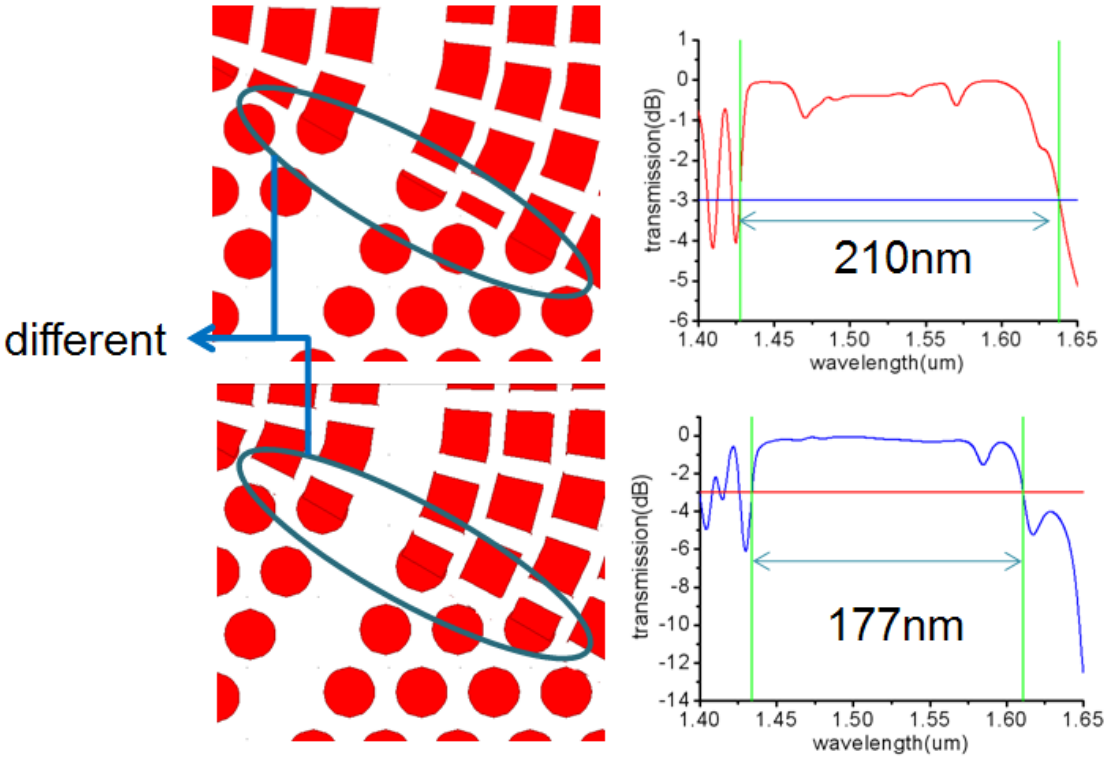

Fig.2.15 the same waveguide bend angle, the different structure in the end of waveguide bend, the spectra are different

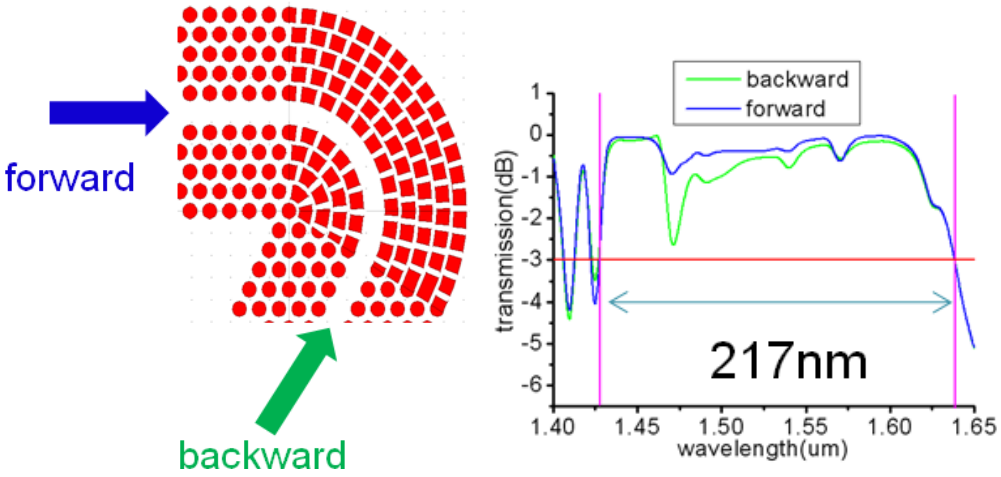

Fig.2.16 the transmission spectra are different when the directions of propagation are different in the same structure

Our design rule will make the different spectrum when the directions of propagation are different, so our device is not reversible. It can't be used in photonic integral circuit. Thus we optimize our structure and make it is reversible. Because the different spectra are causing by different structure at the input and output of waveguide bend region, we want to fix it. For example, the outer layer of 120° waveguide bend is consist of seventeen sectors. We take out two times of θi to be the phase of input and output, and then the remainder angle separate to seventeen sector equally (Fig.2.17 (a)). Althoughθp will be changed after optimizing; it can provide light confinement for our band. Moreover, the transmission spectrum is smoother after optimizing (Fig.2.17 (b)).

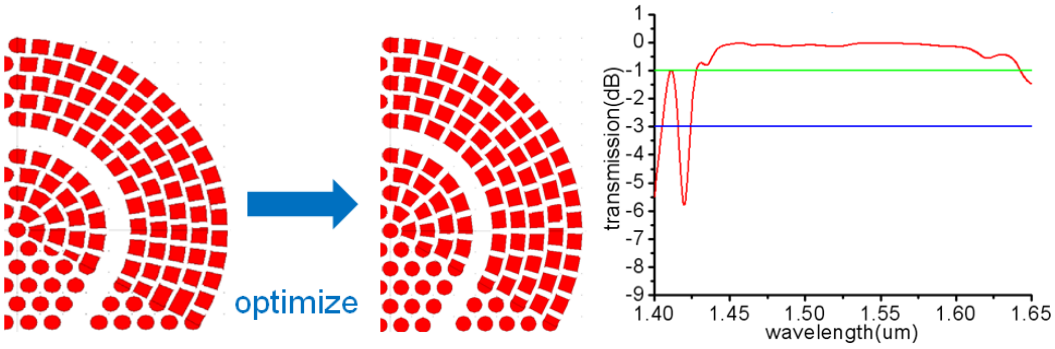

(a) (b)

Fig.2.17 (a) optimize the structure of waveguide bend (b) transmission spectrum after optimizing

Finally we can see the transmission spectra at 120°, 100° , 70° waveguide bend and different propagation direction. It is shown in Fig.2.18. The transmission spectra are almost the same in different angle and the different propagation direction

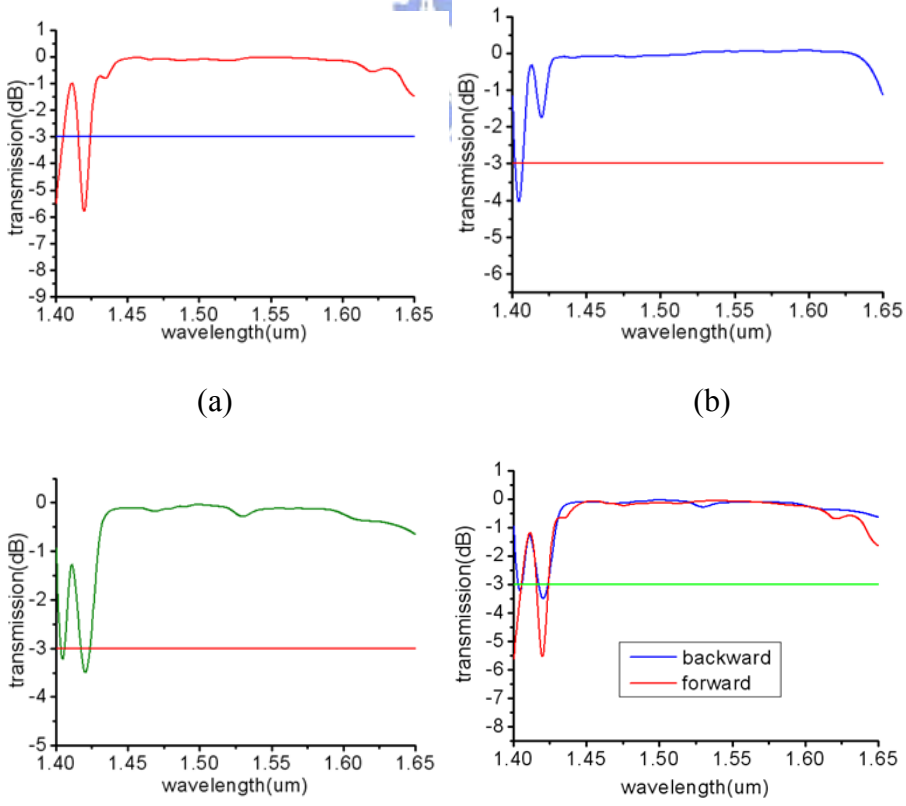

(a) (b)

(c) (d)

Fig.2.18 waveguide bend at (a)120° (b) 100°(c) 70°(d) different propagation direction

Chapter 3. Fabrication and Measurement

3.1. Fabrication processes of active and passive device on membrane structure

Here, we will introduce the fabrication processes of InP-based and GaAs-based membrane structure for active and passive device, respective. In chapter 2, we demonstrate the different propagation direction causing different transmission properties, and backward propagation before optimizing appears a high reflection wavelength at 1470nm. In Z-type structure, this property can make light resonance between two waveguide bend regions, even if lasing. In the other word, we can pump light between two waveguide bend regions and the resonance wavelength can propagate from the waveguide. It is also useful in photonic integral circuit. Furthermore, we also fabricate our design on GaAs-based device and observe the spot light from output port to prove light can transmit in waveguide bend.

The structure of the InP-based wafer is shown in Fig.3.1. The epitaxial structure is InGaAsP/InP multi-quantum wells (MQWs). Four layer 10nm 0.85% compressively-strained InGaAsP quantum wells and three layer 20nm unstrained InGaAsP barrier layers will be alternatively grown on the InP substrate. The photoluminescence (PL) spectrum of the MQWs is centered at the wavelength of 1550nm. The 60nm InP cap layer is used to protect MQWs from destruction during dry etching processes.

The epitaxial structure of GaAs-based wafer is shown in Fig.3.2. The GaAs core take as membrane and its thickness is 220nm to make single mode in the vertical direction.

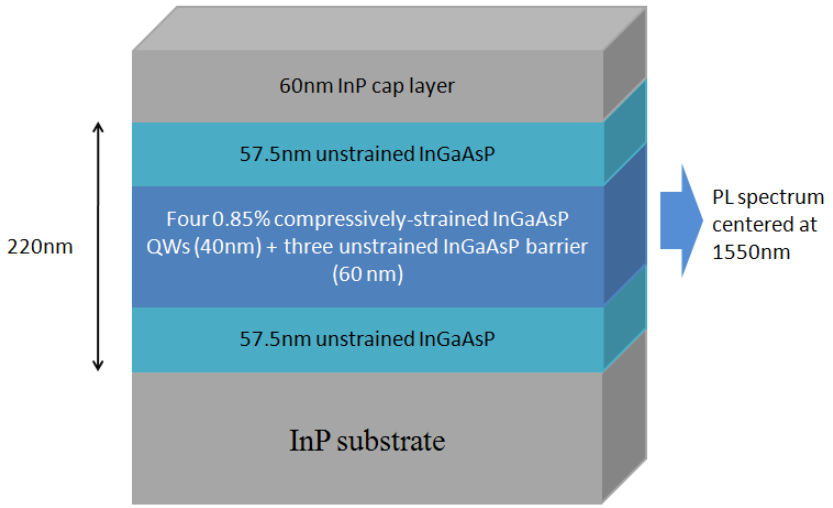

Fig.3.1 The epitaxial structure of InGaAsP/InP MQWs wafer

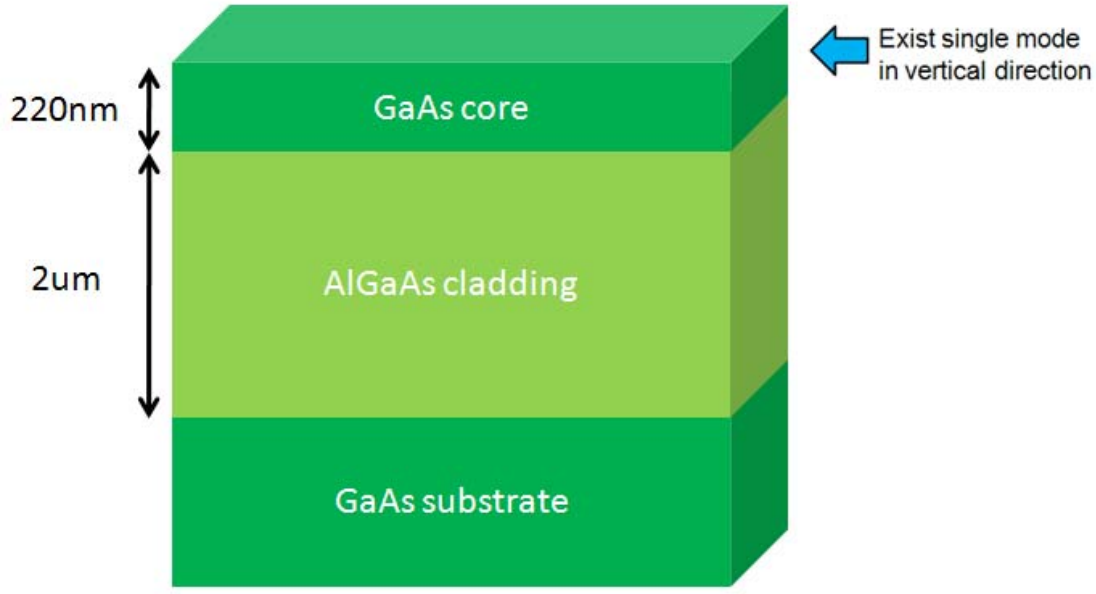

Fig.3.2 The epitaxial structure of GaAs wafer

The fabrication processes of InP can be divided into seven steps as shown in Fig.3.3. First, we use plasma-enhanced-chemical-vapor-deposition (PECVD) with $SiH_4/NH_3/N_2$ mixture gas to deposit 140nm SiN which is served as the hard mask layer. Second, 300nm Polymethylmethacrylate (PMMA) is spin-coated on the SiN layer, and then JEOL 6500 electron-beam (E-Beam) lithography system is employed to define the photonic crystal (PC) pattern. After defining the PC pattern, we use

MIBK/IPA mixture solution to develop it. Third, PC pattern is transferred into the hard mask, MQWs, InP substrate by a series of dry etching processes. We employ the Inductively Coupled Plasma Reactive Ion Etching dry (ICP/RIE) etching system to do this process. Fourth, we use HCl/H_2O mixture solution to undercut the InP substrate at room temperature less than 4°C for 10 minutes depended on the length of device and area of window. Some details of recipe for dry etching step are listed in the Table 3

Step	SiN etch	PMMA remove	InP etch
Gas1(sccm)	O2 5	O2 100	Cl2 21.5
Gas2(sccm)	CHF3 50		H2 25
Gas3(sccm)			CH4 35.5
ICP power(W)			1000
RF power(w)	150	200	85
Pressure(mT)	55	100	4
Temperature(℃)	20	20	150
He(sccm)			10
Time	2'	20"	1'45"

Table 3

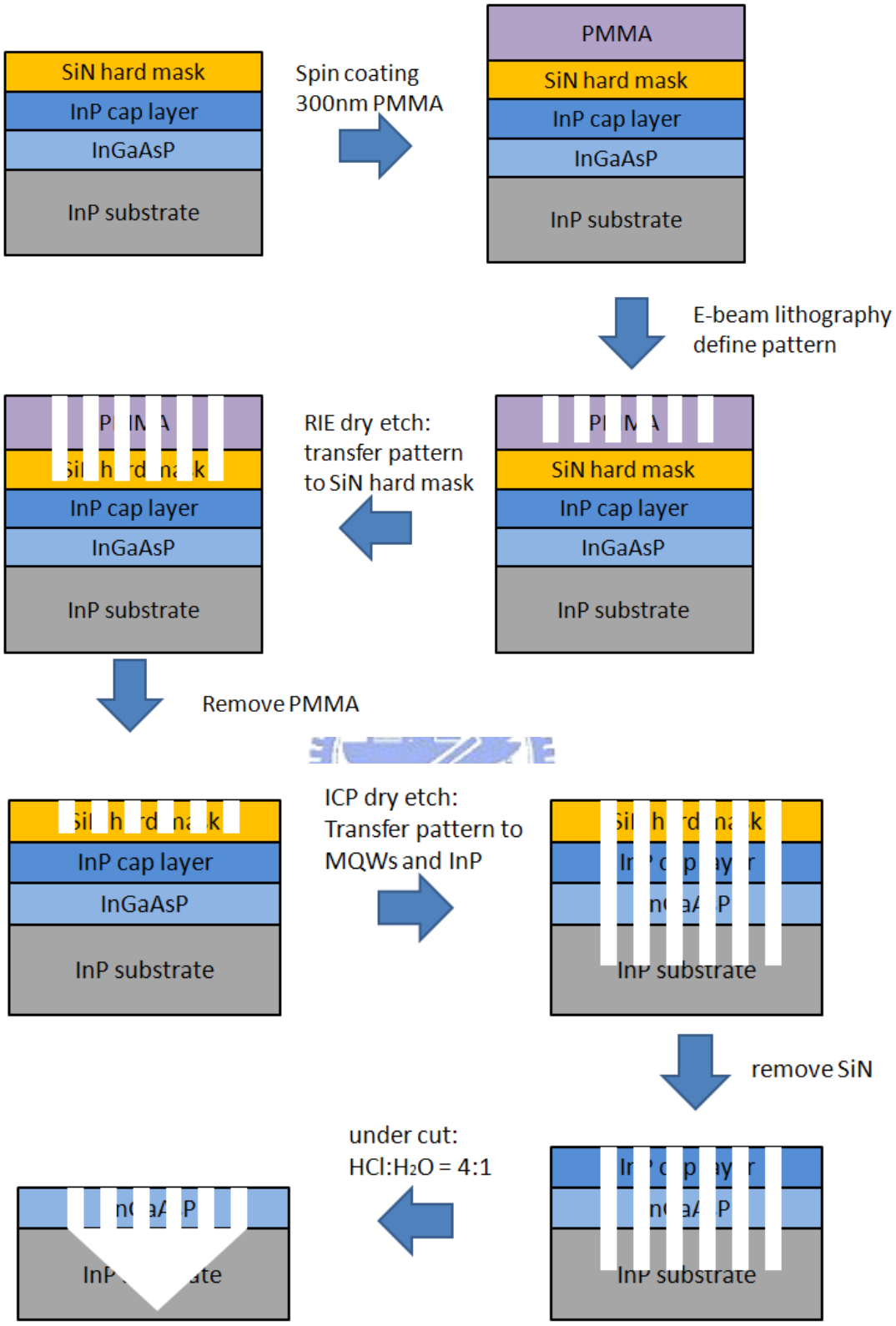

Fig. 3.3 the flow path of fabrication process for membrane structure of InP

And then, the fabrication process of GaAs is similar to InP. Only replace InP etch to GaAs etch and undercut process replace HCl/H_2O mixture solution to H_2PO_3/ H_2O mixture solution. The detailed recipe is shown in Table 4

Step	GaAs etch
Gas1(sccm)	Ar 25
Gas2(sccm)	$SiCl_4$ 7
Gas3(sccm)	
ICP power(W)	350
RF power(w)	40
Pressure(mT)	2
Temperature(℃)	20
He(sccm)	7
Time	1'50"

Table 4

3.2. CAD design and SEM picture

Before the fabrication process, we use CAD tool to layout our design pattern. Fig.3.4 show the CAD design for active and passive device. In order to enhance the ratio of undercut, the windows in pattern of active device are important. The size of window is considered. If the window size is too large, ratio of undercut will be faster. But the nearest hole of photonic crystal will enlarge due to proximity effect of E-beam lithography. If the window size is too small, ratio of undercut will be slower, the time for undercut will be longer and MQWs maybe destroy. Because of undercut of GaAs is isotropic, we don't need design windows in passive device.

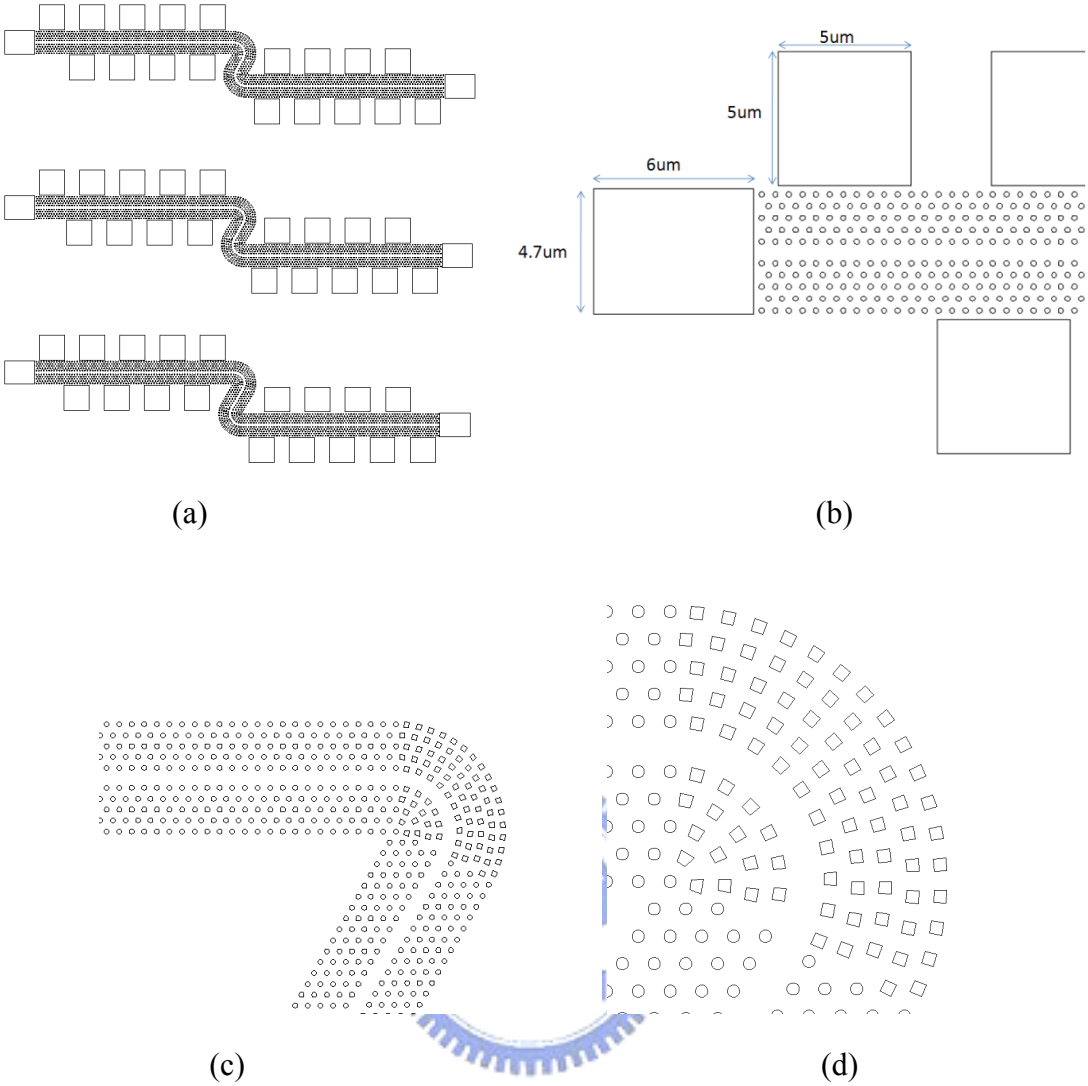

Fig.3.4 (a) CAD design for active device (b) the window design for CAD of active device (c) CAD design for passive device (d) the bend region

Then, we will show the SEM of success device. Fig.3.5 and Fig.3.6 show active and passive device, respectively.

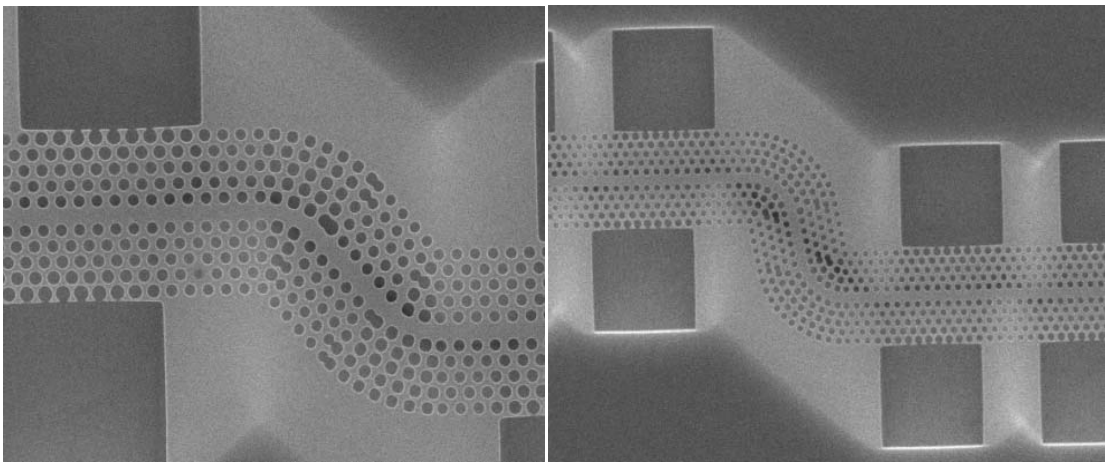

(a) (b)

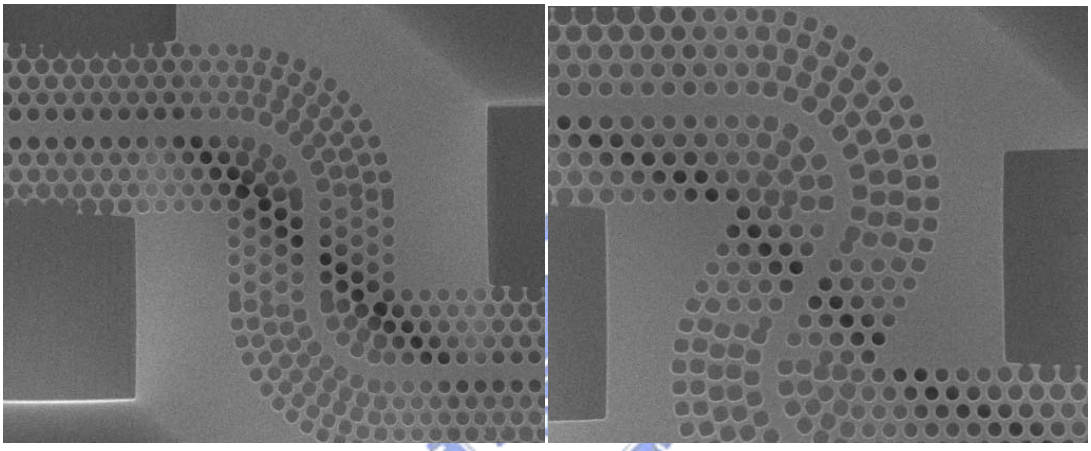

(c) (d)

Fig.3.5 SEM image of active device (a) 50° (b) 80° (c) 90° (d) 120°

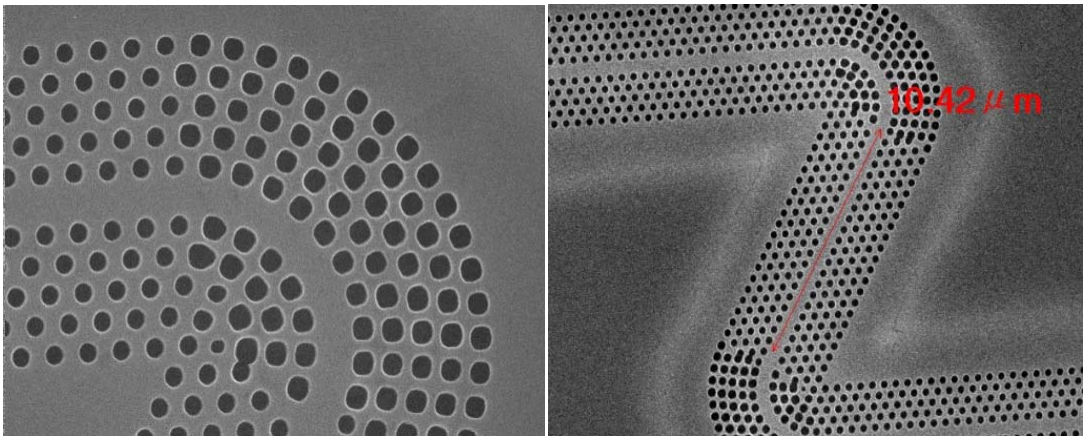

(a) (b)

Fig.3.6 SEM image of passive device (a) bend region (b) 120° Z-type

3.3. Measurement system

In this section, we will introduce our measurement system. Because our devices are fabricated on active and passive substrate, our measurement system divides to two parts. Firstly, we introduce measurement system for active device. The illustration of measurement system for active device is shown in Fig.3.7

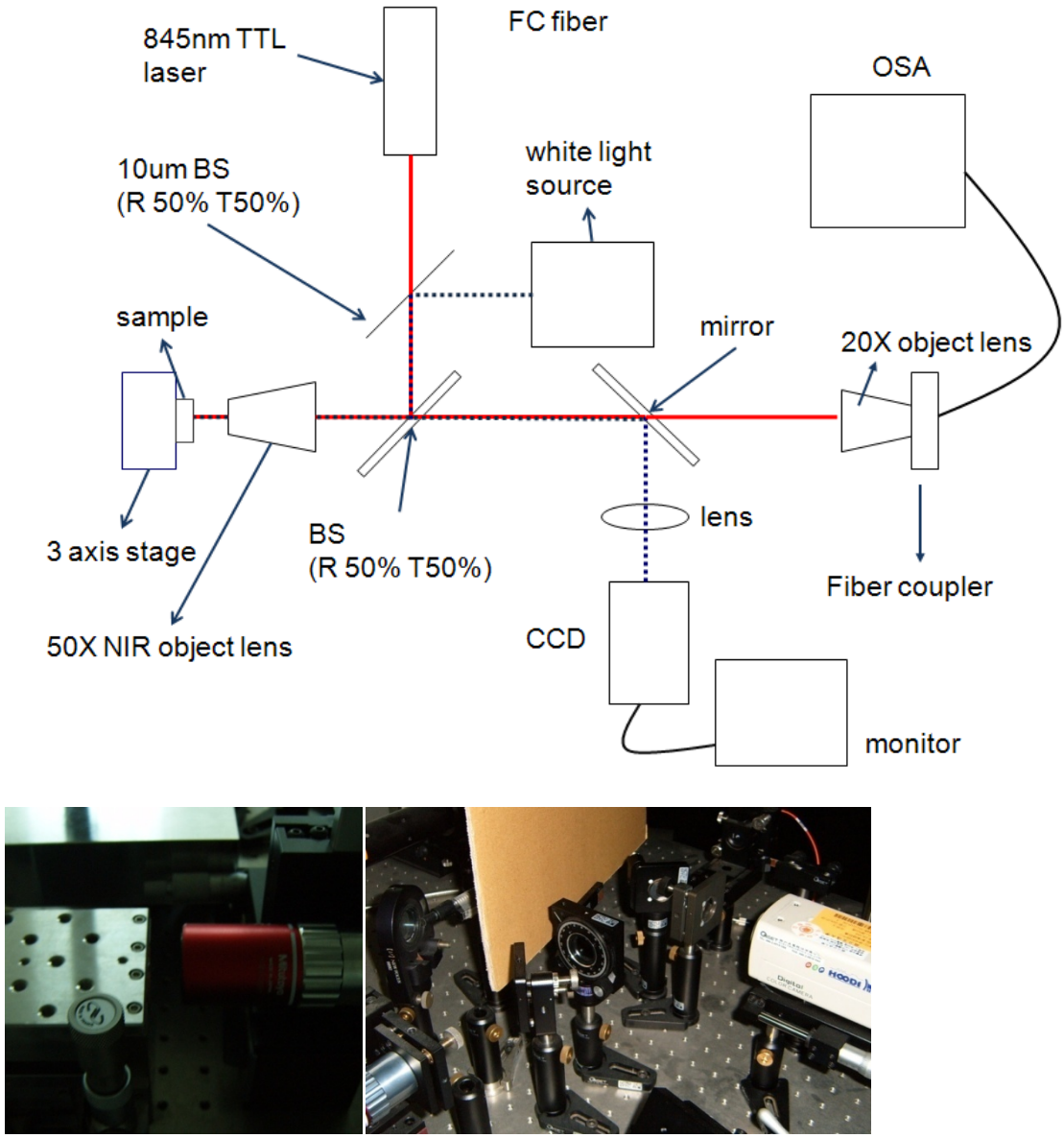

Fig.3.7 The configuration of active device measurement system

The TTL 845nm laser with 0.5% duty cycle is served as an exciting source. The laser beam accompanied with white light source pass through the 50/50 beam splitter, half of laser beam will go into IR camera and form the image, the other one will be focused on the sample by 50X objective lens. The emission has two directions. The vertical emission passes through the 50X objective lens in opposite direction of input laser beam, and directly goes into fiber coupler. The resonant spectrum is analyzed by the optical spectrum analyzer (OSA).

Then, the measurement system for passive device is shown as Fig.3.8. The tunable laser (HP 8168, wavelength from 1475nm~1590nm) pump laser and couple to taper fiber. The taper fiber couple to our sample and observe by micro PL-1. Then moving 2-axis stage let output port to focus on micro PL-2. The output wavelength and intensity are analyzed by OSA.

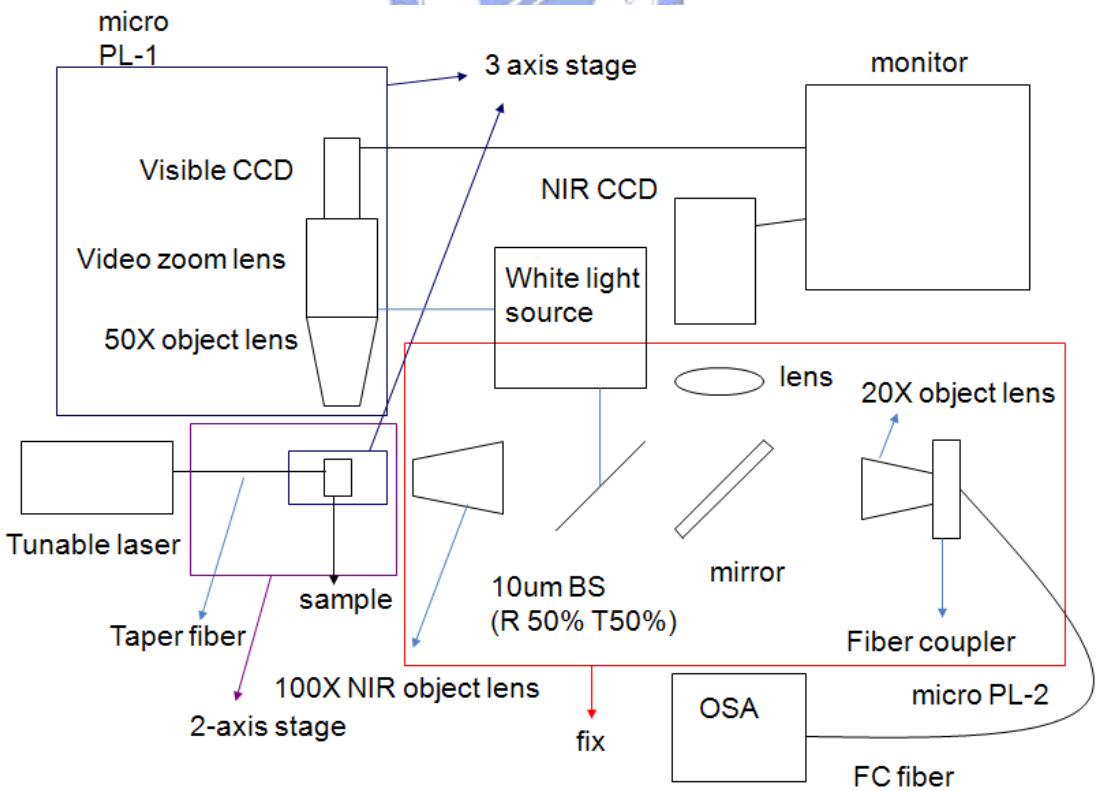

(a)

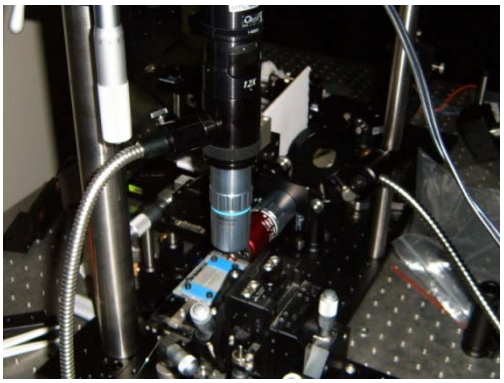

(b)

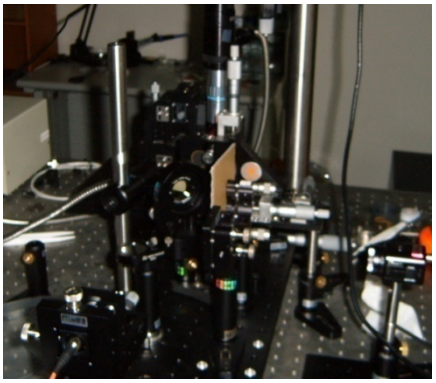

(c)

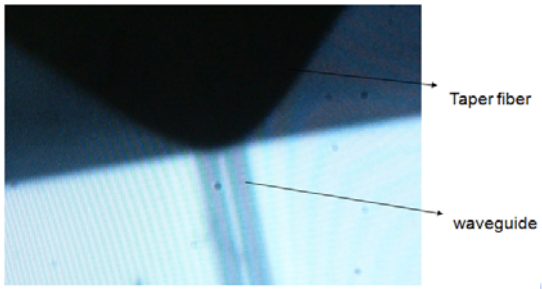

(d)

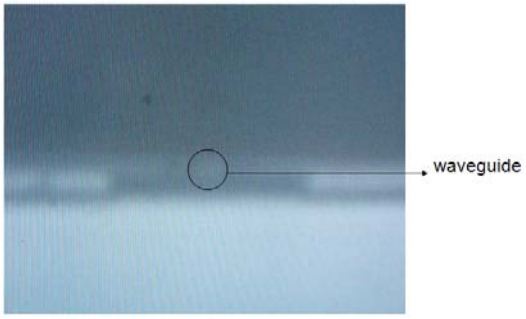

(e)

Fig.3.8 (a) The configuration of passive device measurement system (b) input region (c) output region (d) taper fiber couple to input waveguide (e) output port focus on micro PL-2

3.4. Measurement result

Firstly, we measure the lasing between bend and bend. We measure 120° waveguide bend, and the lasing wavelength of 120° Z-type bend is 1473nm (See Fig.3.9(b)) and *Q* factor is about 1000. Waveguide length between two bend is 9 periods. We compare with simulation. Backward propagation is also high reflection at 1470nm (red circle in Fig.3.9(c)) and the reflection and *Q* are direct proportion. So we can fine tune the waveguide bend structure to achieve high-Q.

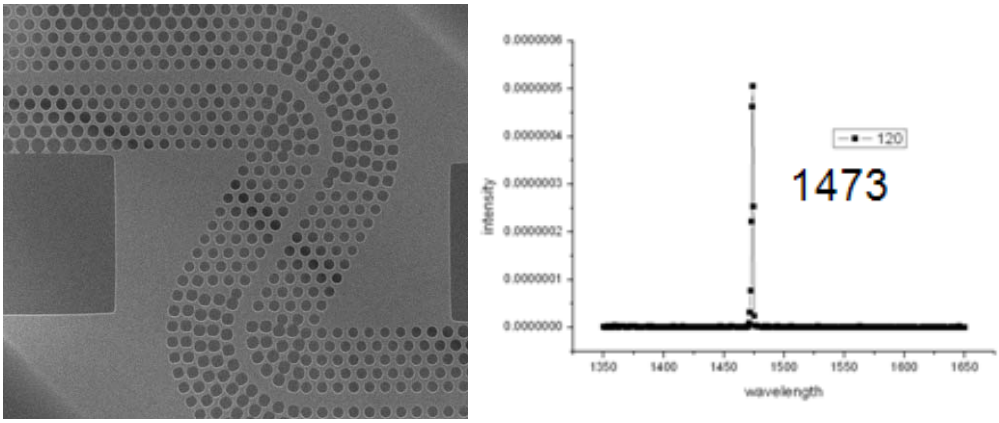

(a) (b)

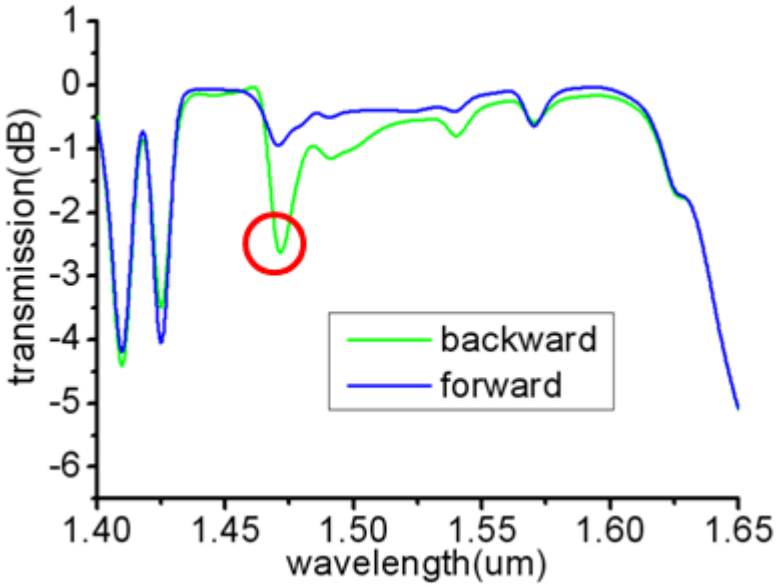

Fig.3.9 (a) SEM of 120° Z-type bend (b) the lasing peak at 1473nm (c) high reflection at 1470nm

And then we also observe if light can propagate in waveguide bend. Before observing we must be seen if the facets of input and output port are smooth. The SEM images are shown in Fig.3.10 and it is clear that the facets are smooth. Next, we align incident light by NIR CCD. The images are show in Fig.3.11 and the pump wavelength is 1550nm. We can see the spot light are different when the taper fiber is aligned or not aligned. After the taper fiber is aligned, we can observe the spot light at

the output port (Fig 3.12). It represents the light actually propagate in waveguide bend.

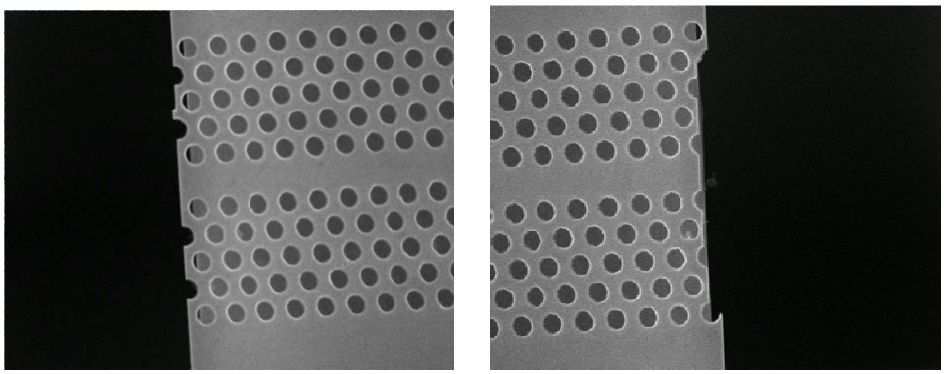

(a) (b)

Fig.3.10 the facet of (a) input port (b) output port

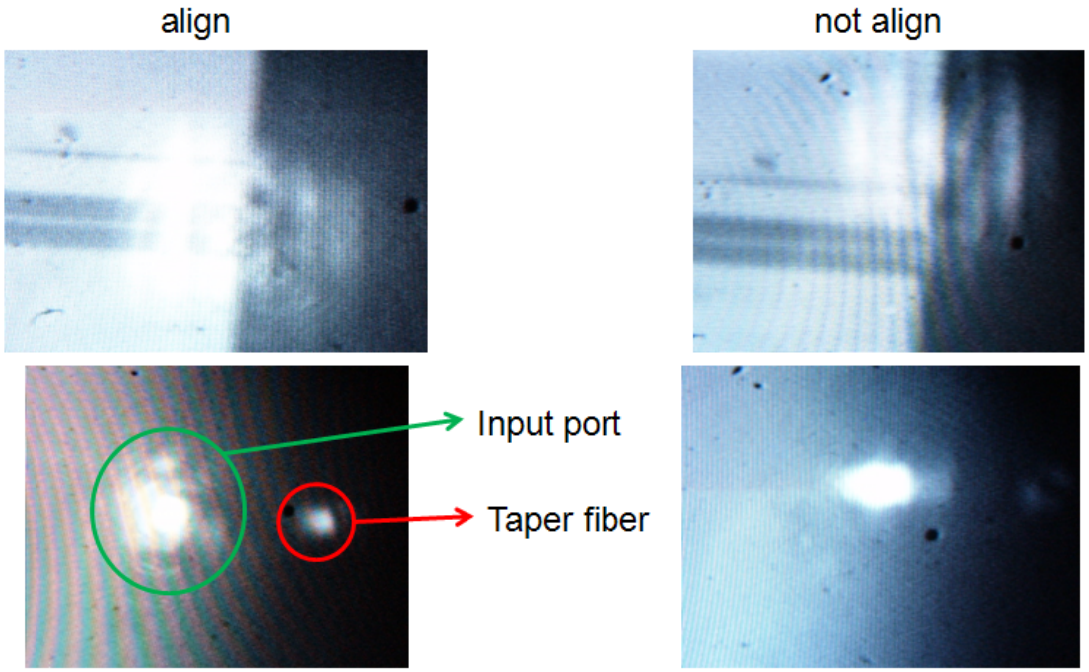

Fig.3.11 different between the taper fiber is aligned or not aligned

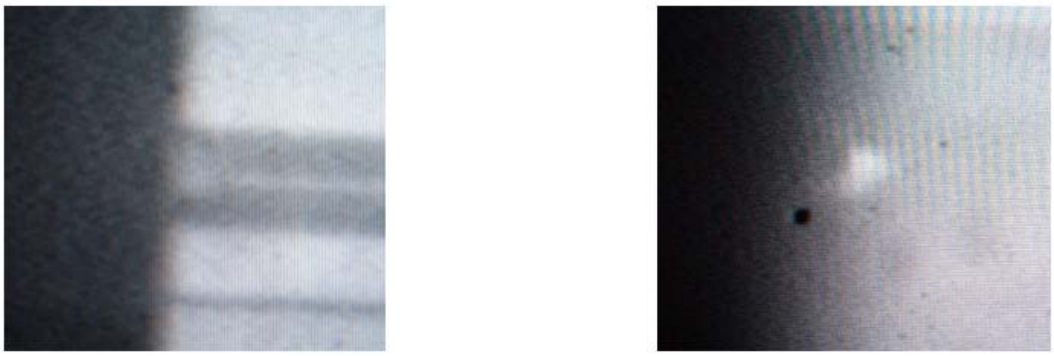

Fig.3.12 CCD image when we focus on visible and communication wavelength

3.5. Conclusion

In this chapter, we fabricate our device on active and passive wafer and measure it. Then we compare measurement result and simulation. In active device, the lasing peak can be measured, and its Q-factor is very low. It means our device in the bend region with low reflection. In the other word, we can fine tune the parameter of bend region, and let its reflection very high. Then we can get a hetero-structure with high Q-factor. Moreover we also observe light spot at output port. It can prove that light can transmit in waveguide bend.

Chapter 4. Conclusion and Future work

4.1. Conclusion

We have proposed a novel structure of waveguide bend by combining circular photonic crystal and annular bragg reflector. In this thesis, we tune the waveguide width to achieve not only broad bandwidth (~200nm) but also around communication. And solve the phase of sector causing different transmission spectrum. Our device is available to arbitrary waveguide bend. It is helpful to photonic integral circuit. Moreover, our device is not only broadband waveguide but also a cavity if we fine tune the structure of bend region.

In the measurement, we setup a measurement system for passive waveguide. And we can observe spot light at input and output ports by NIR CCD to confirm that the light can propagate in waveguide bend actually. In active device, we observe a lasing peak at 1473nm. It is match with high reflection in backward propagation. So our structure is not only a waveguide bend but also a cavity after fine tune.

4.2. Future work

In this thesis, we observe a lasing peak at 1473nm when the length between bend and bend is nine periods. We want to know if the lasing peak be changed while we increase length between bend and bend. Moreover, we will fine tune measurement setup. Because optical loss in micro-PL2 system is too large to measurement transmission spectrum. We consider measuring transmission spectrum by lens-fiber to prevent optical loss in micro-PL2.

Reference

[1] E. Yablonovitch, “Inhibited Spontaneous Emission in Solid-State Physics and Electronics”, Phys. Rev. Lett. 58, 2059-2062, 1987

[2] S. John, “Strong localization of photons in certain disordered dielectric superlattices”, Phys. Rev. Lett. 58 2486-2488, 1987

[3] J. D. Jounnaopoulos, R.D. Meade and J. N. Winn, “Photonic crystals-Molding the Flow of Light”, 1995

[4] Lord Rayleigh, Philosophical Magazine 24, 145-159, 1887

[5] Lord Rayleigh, Philosophical Magazine 26, 256-265, 1888

[6] Y. Lin, E. Chow, V. Hietch, P. R. Villeneuve, J. D. Jounnaopoulos, “Experimental Demonstration of Guiding and Bending of Electromagnetic Waves in a Photonic crystal,” Science 282 pp. 274-276, 1998

[7] A. Talneau *et al*.,” Photonic-crystal ultrashort bends with improved transmission and low reflection at 1.55 mm” Appl. Phys. Lett., Vol. 80, No. 4, 28 January 2002

[8] S.Noda *et al*, “Wider bandwidth with high transmission through waveguide bends in two-dimensional photonic crystal slabs”Appl. Phys. Lett., Vol. 80, No. 10, 11 March 2002

[9] A. Talneau *et al*, “Low-reflection photonic-crystal taper for efficient coupling between guide sections of arbitrary widths”OPTICS LETTERS / Vol. 27, No. 17 / September 1, 2002

[10] J. S. Jensen and O. Sigmund3 May 2004 / Vol. 12 No. 9 / OPTICS EXPRESS 1999

[11] Yao Zhang *et al*, “Ultracompact waveguide bends with simple topology in two-dimensional photonic crystal slabs for optical communication wavelengths”Opt. Lett. Vol. 32, No. 7 April 1, 2007

[12] H. Miyazaki *et al*, “High-transmission waveguide with a small radius of curvature at a bend fabricated by use of a circular photonic crystal”May 1, 2005 / Vol. 30, No. 9 / OPTICS LETTERS

[13] S. Xiao, M. Qiu “Study of transmission properties for waveguide bends by use of a circular photonic crystal” Physics Letters A 340 (2005) 474–479

[14] Ziyang Zhang, Min Qiu” Compact in-plane channel drop filter design using a single cavity with two degenerate modes in 2D photonic crystal slabs,” 4 April 2005 / Vol. 13, No. 7 / OPTICS EXPRESS 2596

[15]R. Wilson, T. J. Karle, I. Moerman and T. F. Krauss, “Recirculation-enhanced switching in photonic crystal Mach-Zehnder interferometers,” J. Opt. A: Pure Appl. Opt. 5, S76-S80, 2003

[16]Yu Tanaka, Y. Sugimoto, N. Ikeda, H. Nakamura, K. Asakawa, and KInoue,”Wavelength-Dependent Coupling Characteristics in Two-Dimensional Photonic-Crystal Slab Directional Coupler,” J. J. Appl. Phys. 44, 4971-4974, 2005

[17] M. G. Banaee, A. G. Pattantyus-Abraham, M. W. McCutcheon,G. W. Rieger, and Jeff F. Young” Efficient coupling of photonic crystal microcavity modes to a ridge Waveguide” Appl. Phys. Lett. 90, 193106 2007

[18] Hongliang Ren, Chun Jiang, Weisheng Hu, Mingyi Gao, and Jingyuan Wang”Photonic crystal power-splitter based on mode splitting of directional coupling waveguides” Optical and Quantum Electronics (2006) 38:645–654

[19] D. O’Brien, M.D. Settle1, T. Karle, A. Michaeli2, M. Salib3 and T.F. Krauss” Coupled photonic crystal heterostructure nanocavities” 5 February 2007 / Vol. 15, No. 3 / OPTICS EXPRESS 1229

[20] Hitomichi Takano, Bong-Shik Song, Takashi Asano, and Susumu Noda” Highly efficient multi-channel drop filter in a two-dimensional hetero photonic crystal” 17 April 2006 / Vol. 14, No. 8 / OPTICS EXPRESS 3491

[21] B. S. Song, T. Asano, Y. Akahane, Y. Tanaka, and S. Noda, “Transmission and reflection characteristics of in-plane hetero-photonic crystals,” Appl. Phys. Lett. **85**, 4591-4593 (2004).

[22] Amnon Yariv *et al*, IEEE JOURNAL OF SELECTED TOPICS IN QUANTUM ELECTRONICS, VOL. 11, NO. 2, MARCH/APRIL 2005

[23] Amnon Yariv *et al*, November 15, 2004 / Vol. 29, No. 22 / OPTICS LETTERS

[24] Derek Chang, Jacob Scheuer and Amnon Yariv, 14 November 2005 / Vol. 13, No. 23 / OPTICS EXPRESS 9273

Vita

Chun-Jung Shih was born at 19 August, 1984 in Chiayi City, Taiwan. He received the B.S. degree from Department of Physics, National Central University, Taiwan in 2006. The M.S. degree will be received from Department of Photonics and Display Institute, National Chiao Tung University, Hsinchu, Taiwan in 2008. His research is photonic crystal waveguide arbitrary bending.